International Journal of Modern Physics B
Vol. 23, No. 22 (2009) 4589–4627

DOI: 10.1142/S0217979209053308

World Scientific
www.worldscientific.com

CONFIGURATIONAL ENTROPY IN GENERALIZED LATTICE-GAS MODELS

ANTONIO J. RAMIREZ-PASTOR*,
FEDERICO J. ROMÁ† and JOSÉ L. RICCARDO‡

Departamento de Física, Instituto de Física Aplicada,
Universidad Nacional de San Luis-CONICET, Chacabuco 917,
San Luis 5700, Argentina
**antorami@unsl.edu.ar*
†froma@unsl.edu.ar
‡jlr@unsl.edu.ar

Received 9 January 2009

In this review, we present our recent results concerning accurate calculations of configurational entropy in generalized lattice-gas models. The calculations are based on the use of the thermodynamic integration method. Different applications (or systems) have been considered. Namely, systems in presence of (i) anisotropy, (ii) energetic heterogeneity, (iii) geometric heterogeneity, and (iv) multisite-occupancy adsorption. Total energy is calculated by means of the Monte Carlo simulation. Then the entropy is obtained by using thermodynamic integration starting at a known reference state. In case (iv), the method relies upon the definition of an artificial Hamiltonian associated with the system of interest for which the entropy of a reference state can be exactly known. Thermodynamic integration is then applied to obtain the entropy in a given state of the system of interest. A rich variety of behaviors is found and analyzed in the context of the lattice-gas theory.

Keywords: Lattice-gas theory; configurational entropy; heterogeneous surfaces; multisite occupancy; Monte Carlo simulation.

1. Introduction

Configurational entropy has been continued to be a useful tool in some complex areas of thermodynamics. Thus, computational and analytical accurate calculations of configurational entropy S and free energy F are of major significance to develop a complete picture of generalized lattice-gas thermodynamics of adsorbates. We refer to a generalized lattice-gas as the one in which (1) lateral interactions are asymmetric; (2) the substrate is heterogeneous; and (3) ad-particles are polyatomic, having more than one constituting unit and, hence, occupying several lattice sites.

Recent molecular simulations[1–4] and experimental results[5,6] about the adsorption of different gases in low-dimensional systems have shown clear signals of nonequivalence between particles and vacancies. In fact, adsorption isotherms for

methane, ethane, and others adsorbed on $AlPO_4$-5 and $SAPO_2$-5 are clearly unsymmetrical around half coverage. These phenomena are also visible in the isosteric heat of adsorption. In spite of the obvious significance of these experiments, most developments in adsorption theory preserve a fundamental statistical property, the well-known symmetry particle vacancy.

The main routes to break the symmetry particle vacancy are as follows: (i) to consider three-particle interactions and (ii) to consider pairwise lateral interactions depending on the orientation of the bond. Point (i) has been widely discussed in Ref. 7. This review will restrict attention to lattice systems where the ad–ad interactions are included as in point (ii).

Concerning the substrate, real surfaces generally present inhomogeneities due to irregular arrangement of surface and bulk atoms or the presence of various chemical species, which can significantly affect the main thermodynamics functions. In this sense, adsorption on heterogeneous solid surfaces[8–10] is a widely studied field due to its many applications in science and engineering. Surface heterogeneity is usually separated in energetic and geometric heterogeneity,[8,9] and usually most real solids surfaces present a combination of the two types. However, studying them separately is useful to understand their effects on adsorption of interacting particles. Energetic heterogeneity is manifested through the variation of adsorption energy from one site to another, while geometric heterogeneity is associated with the existence of irregularities in the lattice of adsorbing sites (like variable distance among neighboring sites or variable connectivity), whose effects on adsorption are manifested through adsorbate–adsorbate interactions.

So far energetic heterogeneity has been the most studied in the literature and only marginal attention has been paid to geometric heterogeneity.[8,11,12] However, the latter is perhaps the most relevant one for a wide variety of solids, namely amorphous solids.[13] Amorphous solids are the prototype of systems with quenched geometrical disorder and have been the object of many studies in the field of magnetism, where, on the basis of simple "site-diluted" or "bond-diluted" models like Ising, Heisenberg, and Potts models, interesting questions like the survival of phase transitions and their universality under partial disorder have been discussed and are still posing open problems.[14–17] As it is well-known, adsorption of monomers on a lattice of sites is isomorphic to the Ising model for magnetism in two dimensions. However, while the mentioned studies in magnetism have been developed in absence of an external field, this external field cannot be neglected in adsorption since it is related to the chemical potential of the adsorbate. This fact, in addition to the potential applications, makes the study of adsorption of monomers on lattices with quenched geometric disorder even more appealing.

In the case of adsorption of molecules with multisite occupancy, where adparticles occupy several k contiguous lattice sites (k-mers), the knowledge of the configurational entropy is a difficult matter.[8,18–30] The difficulty in the analysis of the multisite statistics is mainly associated with three factors, which differentiate the k-mers statistics from the usual single-particle statistics. They are as

follows: (i) no statistical equivalence exists between particles and vacancies; (ii) the occupation of a given lattice site ensures that at least one of its nearest-neighbor (NN) sites is also occupied; and (iii) an isolated vacancy cannot serve to determine whether that site can ever become occupied.

For these reasons, it has been difficult to formulate, in an analytical way, the statistics (and kinetics) of occupation for correlated particles. In particular, the lattice-gas properties of k-mers (dimers, trimers, and longer species) are not well-known because of the difficulties arising in the calculation of their thermodynamic functions. Although adsorption of polyatomic species (or the isomorphous problem of binary solution of a polymer phase and a monoatomic solvent) has been addressed long ago in ideal systems, the correct density dependence of configurational entropy of a simple system such as noninteracting dimers on a two-dimensional regular lattice is still unknown. Then, it is necessary to shift to precise numerical calculations in order to obtain free energy and entropy, in discrete systems of interacting particles, for which no exact values of S or F are known.

Following this line of work, accurate computational calculations of configurational entropy in lattice-gas models have been performed in our group.[31–35] The calculations were based on the use of the thermodynamic integration method.[34–39,42] In this paper, we review these recent advances with emphasis in the role and effect of anisotropy, surface heterogeneity, and particle size on the configurational entropy of the adlayer; an aspect that almost none of the thermodynamic adsorption description has ever taken properly and comprehensively into account. The organization of this paper is as follows. The basis of the model and the simulation scheme are presented in Sec. 2. In this framework, four applications are discussed in Sec. 3. Finally, conclusions are drawn in Sec. 4.

2. Basic Definitions

2.1. *The model*

In this section, we describe a generalized lattice-gas model for the adsorption of particles in the monolayer regime. The surface is represented as an regular array of M sites and $m = zM/2$ bonds (being z the connectivity of the lattice), with periodic boundary conditions. A site represents an adsorptive potential minimum, where particles from a gas phase will be allocated upon adsorption, while a bond represents the adsorbate–adsorbate interaction between two particles adsorbed at the connected sites. If a number m' of bonds are eliminated at random from the lattice, a degree of disorder or geometric heterogeneity, $0 \leq \rho \leq 1$, can be defined as $\rho = m'/m$, so that the lattice has a mean connectivity given by $z_{\text{mean}} = z(1-\rho)$. On the other hand, energetic heterogeneity is introduced by considering adsorption sites with a discrete energy distribution of W different energies $\varepsilon_1, \varepsilon_2, \ldots, \varepsilon_W$. Thus, the surface is modeled as a collection of these sites arranged in different topographies.

We address the general case of adsorbates assumed to be linear particles containing k identical units (k-mers), with each one occupying a lattice site. Small

adsorbates with spherical symmetry would correspond to the monomer limit ($k = 1$). The distance between k-mer units is assumed to be equal to the lattice constant; hence, exactly k sites are occupied by a k-mer when adsorbed. In order to describe a system of N k-mers adsorbed on M sites at a given temperature T, let us introduce the occupation variable c_i, which can take the values $c_i = 0$ or 1, if the site i is empty or occupied by a k-mer unit, respectively. The k-mer retains, its structure upon adsorption, desorption, and diffusion. The Hamiltonian of the system is given by

$$H = w \sum_{\langle i,j \rangle} c_i c_j b_{ij} - N(k-1)w + \sum_{i=1}^{M} \varepsilon_i c_i \,, \tag{1}$$

where w is the NN interaction (we use the convention $w > 0$ for repulsive and $w < 0$ for attractive interactions), $\langle i, j \rangle$ represents pairs of NN sites; b_{ij}'s are bond-occupation numbers ($= 0$ if the bond connecting sites i and j are missing, $= 1$ if it is present), and ε_i is the adsorption energy at site i. The term $N(k-1)w$ is subtracted in Eq. (1) since the summation over all the pairs of NN sites overestimates the total energy by including $N(k-1)$ bonds belonging to the N adsorbed k-mers.

2.2. *TIM in canonical ensemble*

The advantages of using Monte Carlo (MC) simulation to calculate thermal averages of thermodynamic observables are well-known.[36] The estimation of certain quantities, such as total energy, energy fluctuations, correlation functions, etc., is rather straightforward from averaging over a large enough number of instantaneous configurations (states) of a thermodynamic system. However, free energy and entropy, in general, cannot be directly computed. In order to calculate free energy and entropy, various methods have been developed, namely, TIM,[34–42] Ma's method of coincidence counting of states along the trajectory in phase space,[43] "stochastic models" method of Alexandrowicz,[44] "local states" method of Meirovitch,[45] "multistage sampling" and "umbrella sampling" of Valleau *et al.*,[46–49] method of Salsburg,[50] method of Yip *et al.*[51] (which is an optimized combination of coupling parameter and adiabatic switching formalisms), etc.

Among the methods mentioned in the previous paragraph, the TIM is one of the most widely used and practically applicable. In the following, we briefly describe this method.

Given a lattice gas of N interacting particles on a regular lattice with M sites at temperature T, from the basic relationship

$$(\partial S/\partial T)_{N,M} = \frac{1}{T}(\partial U/\partial T)_{N,M} \,, \tag{2}$$

it follows

$$S(N, M, T) = S(N, M, T_o) + \int_{T_o}^{T} \frac{dU}{T} \,, \tag{3}$$

where U is the mean total energy of the system.

$S(N, M, T)$ is readily calculated if $S(N, M, T_o)$ (reference state) is known, given that the integral in the second term can be accurately estimated by MC simulation. In practice, the calculation of S in a reference state can be rigorously accomplished by analytical methods only in a very few cases. Although the entropy of some particular states is trivially known (for example, $S_{N\to 0} \to 0$), this is often computationally inconvenient since it would require the simulation of a thermodynamically open system to get the entropy of a state at finite density. Alternatively, integration can be carried out through a thermodynamic path of a closed (mechanically isolated) system along a constant density path, if a proper reference state is defined for which $S(N, M, T_0)$ can be directly computed.

In the case of monomers ($k = 1$), the determination of the entropy in the reference state is trivial. In fact, for a monoatomic lattice gas

$$S(N, M, T_o = \infty) = k_B \ln \binom{M}{N}, \tag{4}$$

where k_B is the Boltzmann constant. The last equation holds for any finite value of the lateral interactions between the ad-particles. Thus, Eq. (4) will be used to calculate the reference state in the cases discussed in Secs. 3.1, 3.2 and 3.3.

Since $S(N, M, \infty)$ cannot be exactly calculated for k-mer adsorption ($k \geq 2$) by analytical means, in the following we present a general numerical methodology to obtain the entropy of generalized lattice gas in a reference state.

If an artificial lattice gas is defined from the system of interest (henceforth referred to as the original system) such that it fulfills the condition

$$S_A(N, M, \infty) = S(N, M, \infty)\,, \tag{5}$$

$$S_A(N, M, 0) = 0\,. \tag{6}$$

Then, the integral in Eq. (3) can be separated into two terms. Thus,

$$\begin{aligned} S(N, M, T) &= S_A(N, M, \infty) + \int_{\infty}^{T} dU/T \\ &= S_A(N, M, 0) + \int_{0}^{\infty} dU_A/T + \int_{\infty}^{T} dU/T \\ &= \int_{0}^{\infty} dU_A/T + \int_{\infty}^{T} dU/T\,, \end{aligned} \tag{7}$$

where U_A and U are the mean total energy of the artificial and original system, respectively (both integrals can be evaluated by MC in the canonical ensemble). The general definition of the artificial reference system follows.

Let us assume the original system to be a discrete system of N particles on M sites with Hamiltonian $H(N, M, i) = U(N, M, i)$ $i \in \gamma$, where $U(N, M, i) =$ finite $\forall i \in \gamma$ is the potential energy in the ith configuration among the set of accessible configurations γ. The original system can only have access to those configurations

within γ, the total amount of configurations in γ is $G_T(N,M)$ (in a lattice gas of N monomers with single-site occupancy of M sites, $G_T(N,M) = M!/[N!(M-N)!)]$).

The Hamiltonian for the artificial system, H_A, follows from:

Definition 1. H_A is defined as $H_A(N,M,j) = U_A(N,M,j) =$ finite $\forall j \in \gamma_A$, where U_A and $\gamma_A = \gamma$ have analogous meanings to those given above for U and γ, respectively. The equalities ensure that the set of accessible configurations for the original system and the artificial system is equal (although $\gamma_A = \gamma$, the energy of the configurations in the artificial system may be, in general, different from the ones in the original system).

Definition 2. The potential energy of the accessible configurations ($j \in \gamma_A$) for the artificial system takes the following values:

$$\begin{aligned} &U_A(N,M,j_o) = 0\,, \quad && j_o \in \gamma_A\,, \\ &U_A(N,M,j) > 0\,, \quad && j \neq j_o\,, \quad j \in \gamma_A\,. \end{aligned} \tag{8}$$

Definition 2 means that a given configuration (the j_0th) is selected arbitrarily from γ_A and defined as the nondegenerate ground state of the artificial lattice gas; hence, $S_A(N,M,0) = 0$. In practice, the configuration j_0 can be easily defined.

An example for adsorbed dimers follows in order to make this point clear. Let us consider adsorbed dimers on an homogeneous square lattice with $b_{ij} = 1\ \forall \langle i,j \rangle$ and interaction between NN dimer's heads as shown in Fig. 1 (original system). For this system, there is no rigorous expression of $s(N,M,\infty)$ for $N > 0$ in the thermodynamic limit ($N \to \infty$, $N/M \to$ constant).

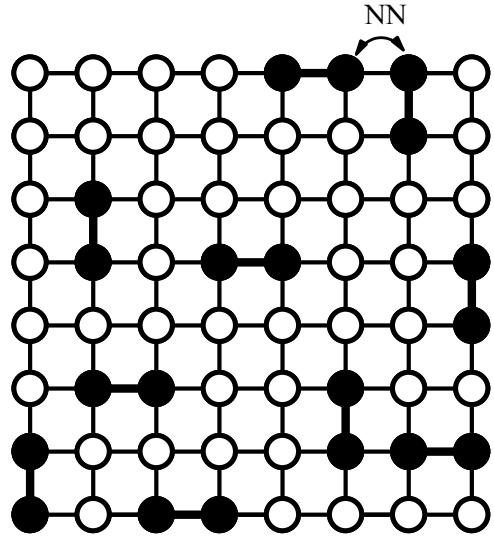

Fig. 1. Dimers ($N = 10$) adsorbed on a square lattice of $M = 64$ sites. Typical nearest-neighbor (NN) units are labeled. This represents the system of interest (original).

To build up an artificial system fulfilling Definitions 1 and 2, we follow the steps:

(i) The number of particles, size, and geometry of the lattice are kept as in the original system.
(ii) The interaction energy between NN units is set to zero.
(iii) An adsorption energy is introduced for the lattice sites (representing, for each site, the interaction between the lattice and the unit of the dimer adsorbed on it in the artificial system), in such a way that two types of sites are defined,

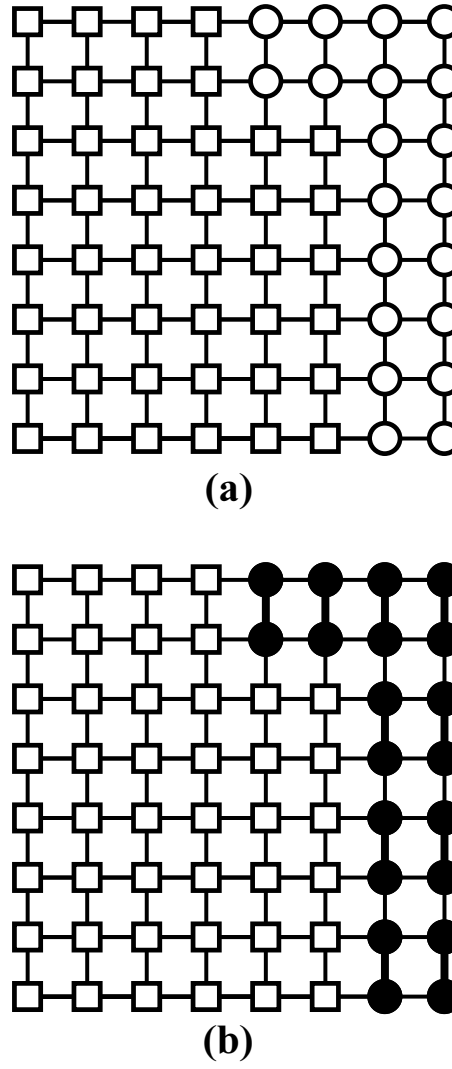

Fig. 2. (a) Square lattice of $M = 64$ sites representing the lattice of the artificial system; strong and weak sites are symbolized by circles and squares, respectively. (b) Configuration of $N = 10$ dimers in the lowest energy state (ground state) according to the artificial Hamiltonian of Eq. (9).

strong and weak, with energies ϵ_S and ϵ_W, respectively, being $\epsilon_S < \epsilon_W$. For N adsorbed dimers, we choose $2N$ strong sites conveniently on the lattice. For instance, in Fig. 2(a) a possible distribution of strong and weak sites is depicted, where circles and squares are sites of energy ϵ_S and ϵ_W, respectively.

(iv) It is assumed that dimers in a particular direction are energetically favored. This is formally handled by introducing a virtual external field such that the interaction energy between the dimers and the field is $w_n = -1$ if the nth dimer is vertically aligned and $w_n = 0$ otherwise (this choice is obviously arbitrary). Care must be taken if periodic boundary conditions are applied to ensure that the state of minimum energy is unique. Then, the Hamiltonian of the artificial system for this example is given by

$$H_A = \sum_{i=1}^{M} \epsilon_i c_i + \sum_{n=1}^{N} w_n \,, \tag{9}$$

where $\epsilon_i = \epsilon_S = -1$ if the site is strong and $\epsilon_i = \epsilon_W = 0$ if the site is weak.

Thus, the ground state of the artificial system is the one shown in Fig. 2(b), which is nondegenerate, giving $s_A(N, M, 0) = 0$.

2.3. *MC simulation*

The calculation of $s(N, M, T)$ through Eq. (7) is straightforward and computationally simple, since the temperature dependence of $u_A(T)$ and $u(T)$ is evaluated at constant coverage for various values of T following the standard procedure of MC simulation in the canonical ensemble (based on the Metropolis scheme[52]).

The thermodynamic equilibrium is reached by the following Kawasaki's dynamics, generalized to deal with polyatomic molecules. The algorithm to carry out an elementary MC step (MCS) is as follows:

Given a square lattice of M equivalent adsorption sites:

(i) Set the value of the temperature T.

(ii) Set the value of the coverage, $\theta = kN/M$, by adsorbing $N = M/2k$ linear molecules onto the lattice, each molecule occupying k adsorption sites.

(iii) A k-mer and a linear k-uple of empty sites are randomly selected, and their positions are established. Then, an attempt is made to interchange its occupancy state with probability given by the Metropolis rule[52]:

$$P = \min\{1, \exp(-\Delta H/k_B T)\} \tag{10}$$

where $\Delta H = H_f - H_i$ is the difference between the Hamiltonians of the final and initial states.

(iv) A k-mer is randomly selected. Then, a displacement to NN positions is attempted (following the Metropolis scheme), by either jumps along the k-mer axis or reptation by rotation around a unity of the k-mer. This procedure (diffusional relaxation) must be allowed in order to reach equilibrium in a reasonable time.

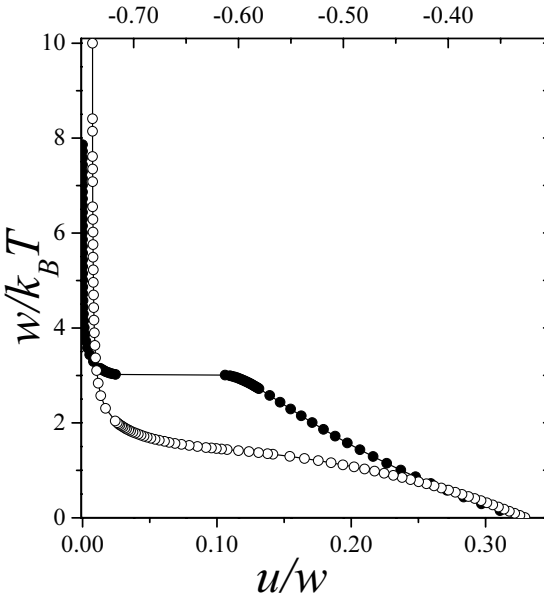

Fig. 3. Mean total energy per site (in units of the interaction energy w) for dimers on a square lattice with nearest-neighbor interaction energy w at fixed coverage $\theta = 0.5$. (a) Open circles and top x-axis correspond to attractive dimers. (b) Full circles and bottom x-axis correspond to repulsive dimers. Simulations were carried out in the canonical ensemble and symbols represent averages over typically $m = 10^6$ MC configurations, after $m' = 10^5$–10^6 equilibration steps.

(v) Repeat steps (iii)–(iv) M times.

The first m' MCS of each run are discarded to allow for equilibrium and the next m MCS are used to compute averages. Then, $u_A(T)$ and $u(T)$ are obtained as simple averages, spline-fitted and numerically integrated. It should be mentioned that $u_A(T)$ and $u(T)$ are calculated by using the Hamiltonians of Eqs. (9) and (1), respectively, in the transition probabilities of the MC procedure. Two typical curves of $1/k_BT$ versus u are shown in Fig. 3, for attractive and repulsive dimers on a square lattice.

The strategy described above is applicable to a wide class of lattice gas systems. However, an efficient exchange MC or simulated tempering method can also be used in order to make the relaxation faster.[53–55] In the following section, we analyze the advantages and accuracy of this methodology in calculating adsorption entropy of generalized lattice gas in one-, two-, and three-dimensional regular lattices.

3. Results and Discussion

We consider here a few applications of the methodology presented in previous sections, namely, analysis of systems in presence of (i) anisotropy, (ii) energetic heterogeneity, (iii) geometric heterogeneity, and (iv) multisite-occupancy adsorption. In the first case (Sec. 3.1), we study interacting monomers adsorbed on one-

dimensional channels arranged in a triangular cross-sectional structure. The couplings are taken to be different in the different lattice directions.[31] In the second case (Sec. 3.2), we address a simple model consisting of a triangular lattice where a fraction of bonds (interactions) is suppressed at random.[32] In the third case (Sec. 3.3), we consider a gas of monomers adsorbed on bivariate heterogeneous surfaces with a characteristic correlation length, l. The bivariate surfaces are composed by two kinds of sites, say weak and strong sites with adsorptive energies ε_1 and ε_2, respectively, arranged in patches of size l with a chessboard structure.[33] Finally, in the fourth case (Sec. 3.4), we study a system of interacting linear molecules (k-mers) absorbed on regular lattices.[34,35]

3.1. *Configurational entropy of interacting particles adsorbed on one-dimensional channels arranged in a triangular cross-sectional structure*

Single-component fluids confined in bundles of carbon nanotubes exhibit a rich variety of phase behaviors.[56–63] Most of these transitions are artifacts because true thermodynamic transitions cannot exist in one dimension for short-ranged interactions. However, a competition between interactions along a single channel (w_L) and a transversal coupling between sites in neighboring channels (w_T) allow one to evolve to a three-dimensional adsorbed layer and lead to genuine thermodynamic phase transitions.[64–69] The principal objective of a theory of phase transitions in confined fluids should be to understand basic physical phenomena. For this purpose, it is necessary to characterize the structures occurring in the adsorbate at critical regime and to determine how these structures are affected by the system geometry, as well as by the interactions (w_L and w_T). Such a description of phase transformations is additionally important from a practical point of view, because porous adsorbents are widely used in a number of relevant technologies (e.g., catalysis, gas separation, and storage).

Numerous experimental and theoretical studies of gas adsorption on carbon nanotube bundles predict the existence of close parallel channels of adatoms when the adsorption takes place (1) inside the nanotubes, (2) in interstitial channels, or (3) in the grooves sites on bundle surfaces.[67,68,70–74] In this context, we present a simplified lattice gas model, where each channel or unit cell has been represented by a one-dimensional line of L adsorptive sites, with periodical boundary conditions. In order to include transverse interactions between parallel neighbor lines, these chains were arranged in a triangular structure of size $R \times R$ and periodical boundary conditions. Under these conditions, all lattice sites are equivalent; hence, border effects will not enter our derivation. The energies involved in the adsorption process are as follows:

(1) ε_0, interaction energy between a particle and a lattice site.
(2) w_L, interaction energy between adjacent occupied axial sites.
(3) w_T, interaction energy between particles adsorbed on NN transverse sites.

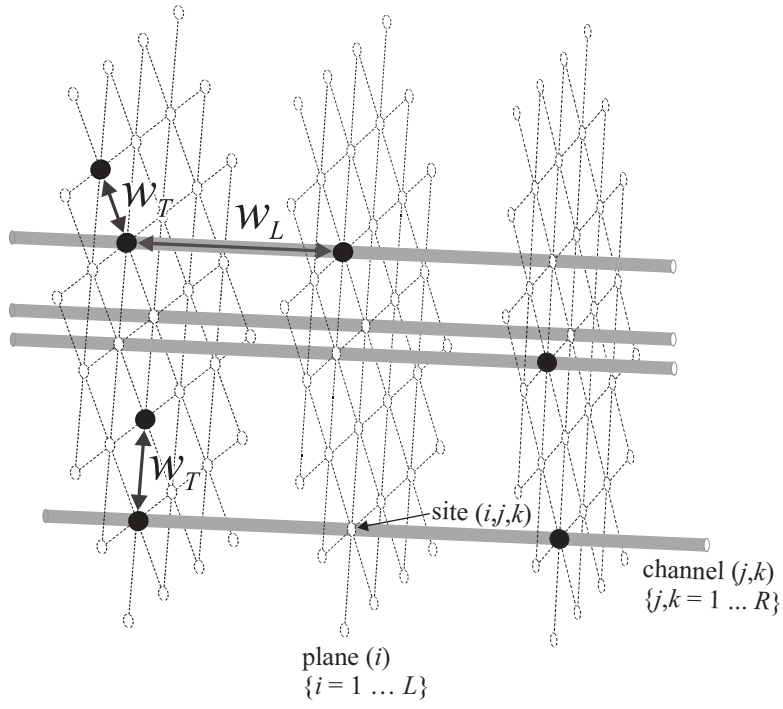

Fig. 4. Schematic representation of the studied system. Black and white circles correspond to occupied and empty sites, respectively.

Thus, the resulting substrate was an anisotropic three-dimensional array of $M = L \times R \times R$ adsorption sites, where each site was surrounded by two "axial" sites along the chain's axis and six "transverse" sites belonging to NN unit cells (see Fig. 4). Then, the Hamiltonian of the system is given by Eq. (1) with $k = 1$, $b_{ij} = 1\ \forall \langle i, j \rangle$, $\varepsilon_i = \varepsilon_0 = 0\ \forall i$ (homogeneous surface), and $w_{ij} = w_L(w_T)$ for axial(transverse) $\langle i, j \rangle$ pairs.

In MC simulations, the system is represented by a unit cell of sites that is repeated periodically. As it was demonstrated by different authors studying adsorption in a porous medium,[64,68] a small cell size is enough to simulate the one-dimensional channels. Then, we choose $L = 96$ in the direction along the axis of the nanotubes. On the other hand, the choice of appropriate sizes in the transversal direction has to be done in such a way that the ordered structures developing at criticality are not disturbed. In our case, lattices with $R = 60$ sites were used. With this lattice size, we verified that finite-size effects, which affect the thermodynamical properties in the case of repulsive interactions at much smaller sizes, are negligible.

We focus on the case of repulsive transversal interaction energy among adsorbed particles ($w_T > 0$). This is far more interesting since, as we shall see, a rich variety of ordered phases are observed in the transversal planes. In addition, repulsive and attractive axial lateral interactions were considered. As it can be easily demon-

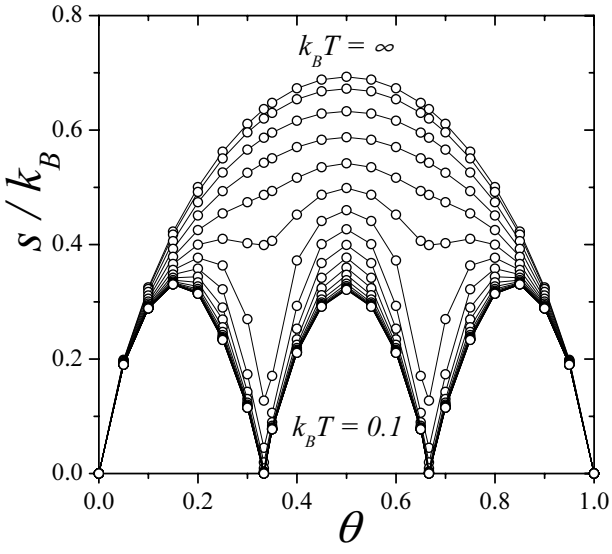

Fig. 5. Configurational entropy per site (in units of k_B) versus the surface coverage for interacting particles adsorbed in one-dimensional channels arranged in a triangular structure with $w_T = 1$ and $w_L = 0$. The curves from top to bottom correspond to values of k_BT ranging from ∞ to 0.1.

strated, the behavior of the system is completely determined by two parameters: w_L/w_T and w_T/k_BT. In our calculations, we can consider $w_T = 1$, in such a way that the system is characterized by two nondimensional parameters w_L and k_BT.

The entropy is obtained from Eqs. (2)–(4). In what follows, the configurational entropy per site s will be used. In order to understand the basic phenomenology, we firstly consider null axial interactions. In this case, successive transversal planes are uncorrelated and the system is equivalent to the well-known triangular lattice.

Figure 5 shows canonical MC simulations of the entropy per site versus the surface coverage for $w_L = 0$. As a consequence of the equivalence particle vacancy, the curves are symmetrical around $\theta = 0.5$. For high temperatures, the overall behavior can be summarized as follows: in the limits $\theta \to 0$ and $\theta \to 1$ the entropy tends to zero. For very low coverage $s(\theta)/k_B$ is an increasing function of θ, reaches a maximum at $\theta = 0.5$, then decreases monotonically to zero for $\theta > 0.5$.

As the temperature is diminished, the entropy decreases for all coverage and develops two local minima at $\theta = 1/3$ and $\theta = 2/3$. In the ground state, $s(\theta = 1/3, T = 0)/k_B = s(\theta = 2/3, T = 0)/k_B = 0$ (see Fig. 6). These singularities provide valuable information about the phase behavior of the system. Precisely, they indicate the formation of ordered structures in the adlayer [$(\sqrt{3}\times\sqrt{3})$ structure at $\theta = 1/3$ and $(\sqrt{3} \times \sqrt{3})^*$ structure at $\theta = 2/3$]. In addition, they are boundaries between three different adsorption regimes: (i) for $0 < \theta < 1/3$, the lattice sites are filled until the $(\sqrt{3} \times \sqrt{3})$ ordered phase is formed on them; (ii) for $1/3 < \theta < 2/3$, this process continues up to the $(\sqrt{3} \times \sqrt{3})^*$ structure is completed; and (iii) for $2/3 < \theta < 1$, the full coverage of the lattice is reached. The results in Figs. 5 and

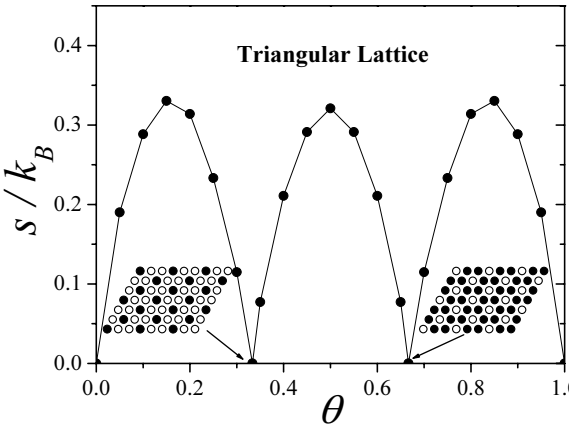

Fig. 6. Configurational entropy per site (in units of k_B) versus the surface coverage for repulsive interacting particles adsorbed in a triangular lattice in the ground state ($w_T = 1$, $w_L = 0$, and $k_BT \to 0$).

6 match previous studies for triangular lattices (see for instance Refs. 75–77) and validate the MC scheme.

We now discuss the case corresponding to attractive axial interactions and different values of k_BT. For the sake of clarity, the analysis will be carried out in two parts. On the one hand, for constant w_L ($w_L = 0; -0.5; -1.00$) and variable values of k_BT ($k_BT = \infty; 0.95; 0.63; 0.47; 0.32; 0.19; 0.10$), each set of curves presents two minima in the entropy as k_BT decreases (see Fig. 7). Same as in Fig. 5, the

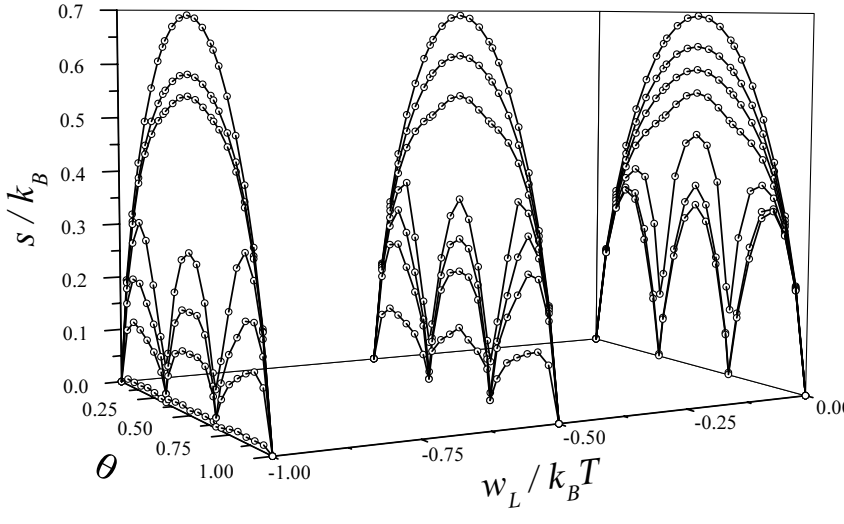

Fig. 7. Configurational entropy per site (in units of k_B) versus the surface coverage for $w_T = 1$ and attractive values of w_L ($w_L = 0; -0.50; -1.00$). For constant w_L, the curves from top to bottom correspond to the following: $k_BT = \infty, 0.95, 0.63, 0.47, 0.32, 0.19$, and 0.1, respectively.

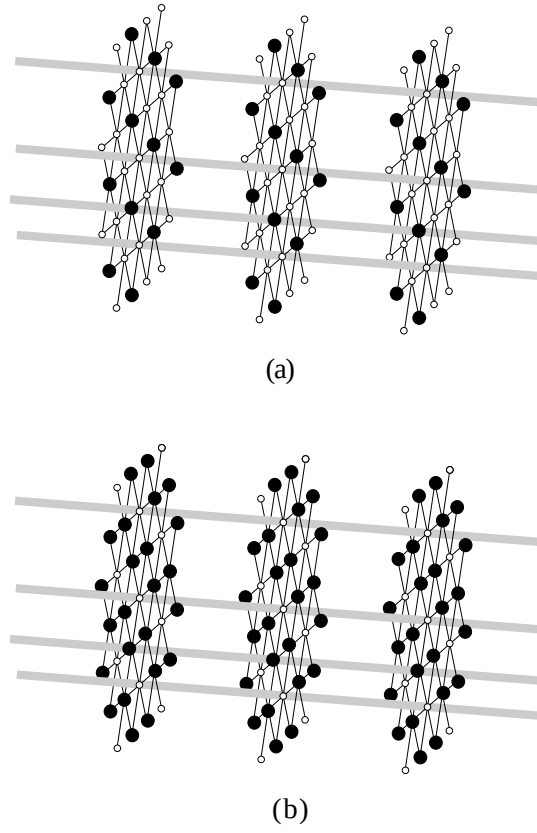

Fig. 8. Snapshots of the adsorbate at (a) $\theta = 1/3$ and (b) $\theta = 2/3$ for interacting particles adsorbed in one-dimensional channels arranged in a triangular structure with $w_T = 1$, $w_L < 0$ and $k_BT \to 0$.

existence of these minima is associated with the formation of ordered structures in the adlayer. In this case, attractive axial interactions favor the formation of pairs of NN adsorbed particles along the nanotubes. Consequently, the $(\sqrt{3} \times \sqrt{3})$ and $(\sqrt{3} \times \sqrt{3})^*$ phases "propagate" along the channels and emerge the structures shown in Fig. 8.

On the other hand, for constant k_BT and variable values of w_L, entropy diminishes over the whole range of coverage as $|w_L|$ is increased. This situation can be clearly visualized in Fig. 9, where a typical case of constant k_BT ($k_BT = 0.32$) and variable w_L ($w_L = 0; -0.25; -0.5; -0.75; -1.00$) is plotted. The position of the total maximum, at $\theta = 0.5$, is independent of w_L, while the position of the local maximum at low (high) coverage tends to $\theta = 0.2$ ($\theta = 0.8$) from the left (right) as w_L tends to -1.

We now turn to repulsive axial interactions, which present an interesting behavior as shown in Fig. 10. Thus, for constant w_L ($w_L = 0; 0.5; 1.00$) and variable

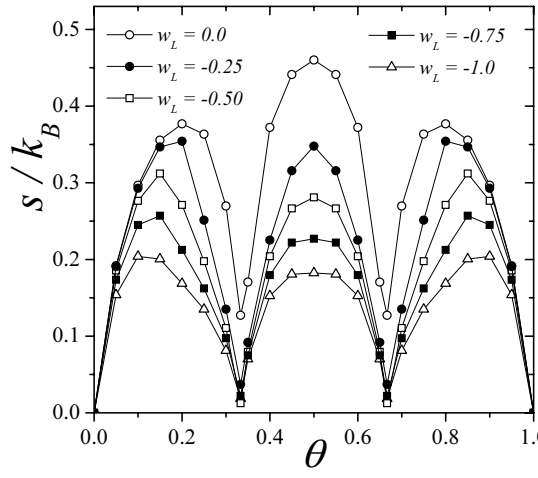

Fig. 9. Configurational entropy per site (in units of k_B) versus the surface coverage for $w_T = 1$, $k_B T = 0.32$ and attractive values of w_L as indicated.

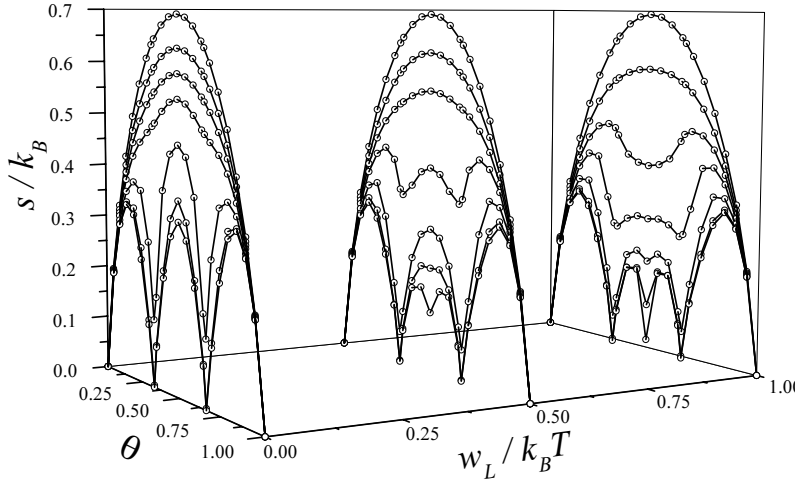

Fig. 10. Same as Fig. 7 for repulsive values of w_L ($w_L = 0; 0.50; 1.00$).

values of $k_B T$ ($k_B T = \infty; 0.95; 0.63; 0.47; 0.32; 0.19; 0.10$), three minima appear in the entropy as T decreases. This can be rationalized as follows: at $\theta = 1/3$ [2/3], a $(\sqrt{3} \times \sqrt{3})$ $[(\sqrt{3} \times \sqrt{3})^*]$ ordered structure is formed in the transversal planes below the critical temperature. In addition, given that $w_L > 0$, particles avoiding configurations with NN axial interactions develop a structure of alternating particles along the channels. Snapshots in Figs. 11(a) and 11(b) correspond to two possible configurations of the phase appearing at critical regime for $\theta = 1/3$ and $\theta = 2/3$, respectively. The degeneracy of such structures is $3.2^{(L-1)}$, and, consequently, $s(\theta = 1/3, T = 0)/k_B = s(\theta = 2/3, T = 0)/k_B = 0$.

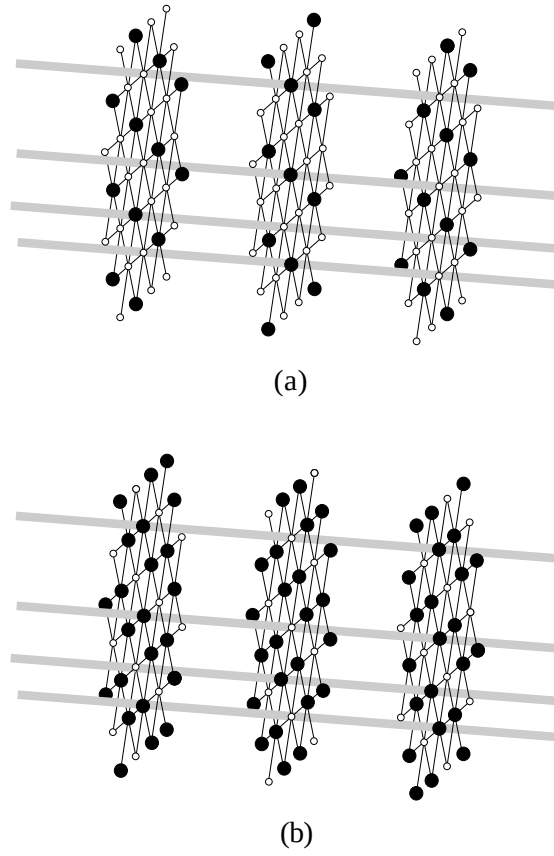

Fig. 11. Snapshots of the adsorbate at (a) $\theta = 1/3$ and (b) $\theta = 2/3$ for interacting particles adsorbed in one-dimensional channels arranged in a triangular structure with $w_T = 1$, $w_L > 0$, and $k_B T \to 0$.

At $\theta = 1/2$ the situation is more complex. In this case, the planes are filled up to $\theta = 0.5$ with mean energy per site equal to $w_T/2$ (each adsorbed particle is surrounded by two occupied NNs in the plane). Then, successive planes are occupied avoiding the formation of monomer–monomer pairs along the nanotubes. In this manner, each transversal plane is surrounded by two complementary planes[a] and the occupation of the channels consists of alternating particles separated by empty sites. Then, the main contribution to the entropy per site comes from the number of different ways, Ω, to arrange the particles on the planes at half coverage with mean energy per site equal to $w_T/2$. This quantity can be obtained from calculations of entropy per site for triangular lattices at $\theta = 0.5$. In these conditions, $\ln \Omega = aR^2$, being $a = 0.32099$ (see Fig. 6). In addition, a factor 2 must be added

[a]A complementary plane is obtained under the simultaneous inversion of all occupation variables ($c_i = 0 \to c_i = 1$ and $c_i = 1 \to c_i = 0$).

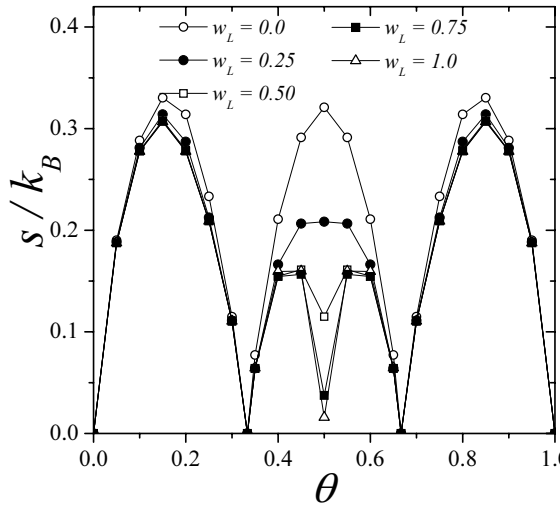

Fig. 12. Same as Fig. 9 for $w_T = 1$, $k_BT = 0.1$ and repulsive values of w_L ($w_L = 0; 0.25; 0.50; 0.75; 1.00$).

in order to include the effect of the complementarity along the channels. Then, in the thermodynamic limit ($L = R \to \infty$), $s_0(1/2) \propto \text{const}\ R^2/(LR^2) = 0$.

On the other hand, Fig. 12 shows the behavior of the configurational entropy as a function of coverage for constant k_BT ($= 0.1$) and variable values of w_L ($w_L = 0; 0.25; 0.5; 0.75; 1.00$). Entropy diminishes over the whole range of coverage as w_L is increased.

The calculations of configurational entropy of the adlayer allowed us to identify a wide variety of structural orderings occurring at $\theta = 1/3$, $1/2$, and $2/3$. A similar behavior was recently reported in Ref. 78 for other properties of adsorption (isotherm and differential heat of adsorption).

Table 1. Critical temperatures corresponding to the critical coverage $\theta = 1/3$, $2/3$, and $1/2$.

	k_BT_c/w_T	
w_L/w_T	$\theta = 1/3, 2/3$	$\theta = 1/2$
−1.00	0.76	—
−0.75	0.67	—
−0.50	0.60	—
−0.25	0.48	—
0.00	0.33	—
0.25	0.42	0.41
0.50	0.49	0.53
0.75	0.54	0.63
1.00	0.59	0.71

In all cases $w_T = 1$.

Finally, the configurational entropy can be used to estimate the critical temperatures corresponding to the critical concentrations $\theta = 1/3$, $1/2$, and $2/3$. For this purpose, the dependence of s/k_B (and its derivative) on temperature was plotted. Some typical cases are shown in Figs. 13 and 14. The inflection point of $s(T)/k_B$ (peak in its derivative) determines the critical temperature. In the studied cases, the calculated values are shown in Table 1. For $w_L = 0$, the critical temperature obtained comes very close to the expected value of $k_B T_c/w_T = 0.3354(1)$ corresponding to the triangular lattice,[55] which indicates the degree of accuracy of the procedure used here.

3.2. *Configurational entropy of interacting particles adsorbed on two-dimensional heterogeneous surfaces*

Increasing interest and efforts have been devoted over decades to developing a deeper understanding of the surface heterogeneity.[8–10] Most of the papers dealing

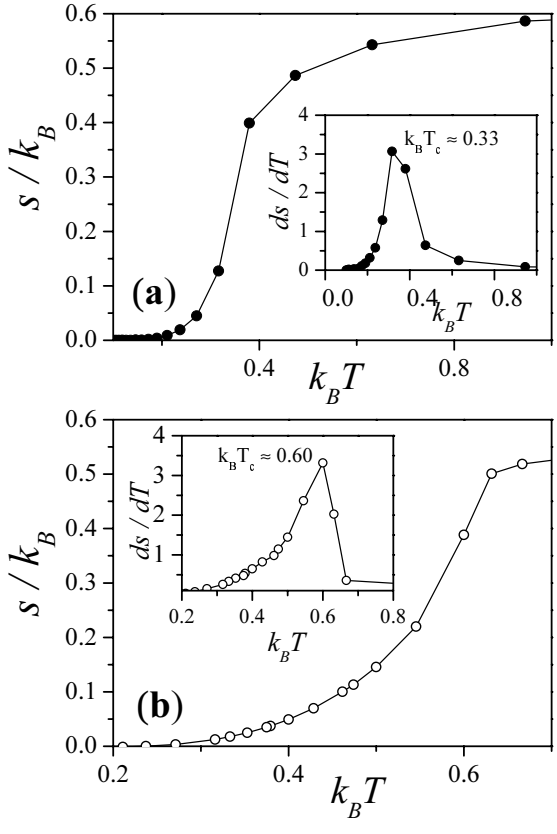

Fig. 13. Configurational entropy per site (in units of k_B) as a function of temperature at the critical coverage. In the inset, we have plotted the corresponding derivative showing a peak in the critical temperatures. (a) $w_T = 1$, $w_L = 0$, and $\theta = 1/3$. (b) $w_T = 1$, $w_L = -0.5$, and $\theta = 1/3$.

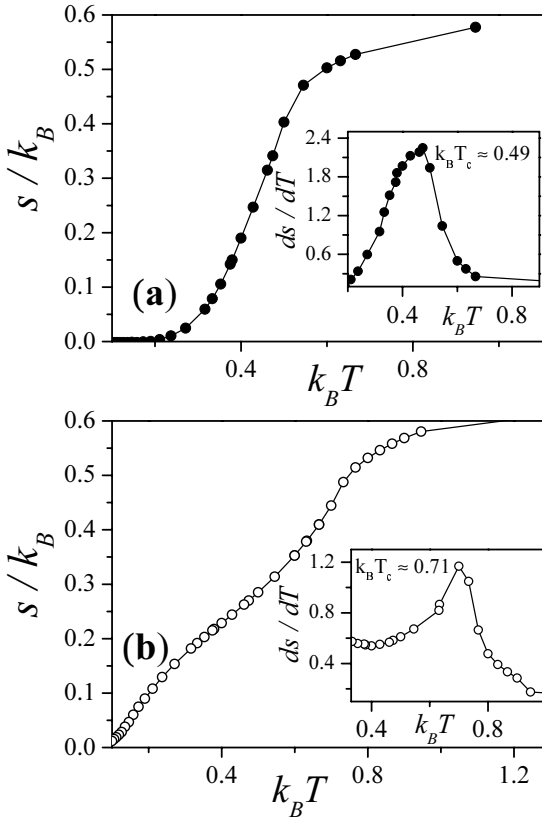

Fig. 14. Configurational entropy per site (in units of k_B) as a function of temperature at the critical coverage. In the inset, we have plotted the corresponding derivative showing a peak in the critical temperatures. (a) $w_T = 1$, $w_L = 0.5$, and $\theta = 1/3$. (b) $w_T = 1$, $w_L = 1$, and $\theta = 1/2$.

with molecular processes on heterogeneous surfaces have been dedicated to the analysis of phenomena such as diffusion,[79] percolation,[80] growth,[81] adsorption isotherms and heats of adsorption,[82,83] multisite occupancy,[84] etc. As it was discussed above, the entropy is much more difficult to evaluate and, in the best knowledge of the authors, there is still a lack of systematic studies on the behavior of the adsorbate's entropy in presence of surface heterogeneity. For these reason, it is of interest and of value to inquire how a specific lattice structure (heterogeneous surface with intermediate correlation) influences the entropy of the adlayer.

In this context, the main objective of the present section is to determine the effects of the surface heterogeneity on the behavior of the configurational entropy of adsorbed interacting particles. We assume that the substrate is represented by a two-dimensional square lattice of $M = L \times L$ adsorption sites, with periodic boundary conditions. Each adsorption site can be either a "weak" site, with adsorptive energy ε_1, or a "strong" site, with adsorptive energy ε_2 ($\varepsilon_1 \leq 0$, $\varepsilon_2 \leq 0$ and $|\varepsilon_1| < |\varepsilon_2|$). Weak and strong sites form square patches of size $l (l = 1, 2, 3, \ldots)$,

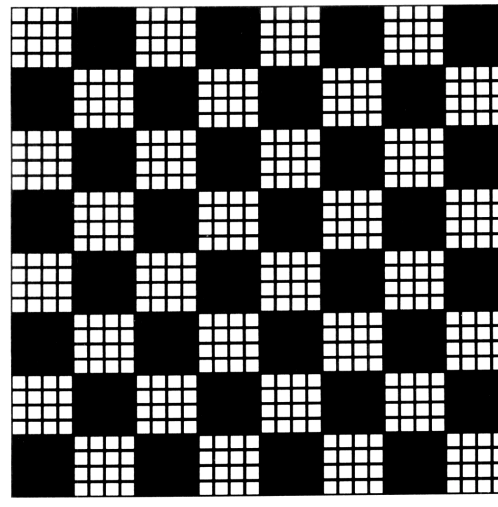

Fig. 15. Schematic representation of a square heterogeneous bivariate surface with chessboard topography. Black (white) symbols represent sites with energy ε_1 (ε_2). The patch size in this figure is $l = 4$.

which are spatially distributed in a deterministic alternate way (chessboard topography), Fig. 15. Then, the Hamiltonian of the system is given by Eq. (1) with $k = 1$, $b_{ij} = 1\ \forall\langle i,j\rangle$ and $\varepsilon_i = \varepsilon_1$ (or ε_2). A special class of this kind of surface has been observed recently to occur in a natural system,[85] although it was already intensively used in modeling adsorption and surface diffusion phenomena.[81–84]

The computational simulations have been developed for square lattices with $L = 144$ (in such a way that it is a multiple of l) and periodic boundary conditions. With this size of the lattice, we verified that finite-size effects are negligible. We focus on the case of repulsive interaction energy among adsorbed particles ($w > 0$). As we shall see, order–disorder transitions can take place in the adsorbate, even if the order can be partially disturbed by heterogeneity. The difference between the energies of the patches has been chosen to be $\Delta\varepsilon = \varepsilon_1 - \varepsilon_2 = 12$ ($\varepsilon_1 = 0$, $\varepsilon_2 = -12$). A high value of $\Delta\varepsilon$ has been considered in order to emphasize the effect of the surface heterogeneity as the temperature is diminished.

We consider in first place a chessboard topography with $l = 12$ (size of each homogeneous patch), and different values of the temperature. Figures 16(a) and 16(b) shows the behavior of the configurational entropy per site, s, versus θ for $w = 1$ ($w = 2$). As a consequence of the equivalence particle vacancy, the curves are symmetrical around $\theta = 0.5$.

For high temperatures, the behavior of s was discussed in Fig. 5 (note that, for $T \to \infty$, the curve of s versus θ does not depend on the lattice geometry). As the temperature is diminished, the entropy decreases for all coverage and develops three local minima at $\theta = 1/4$, $1/2$, and $3/4$. In the ground state, $s(\theta = 1/4, T = 0)/k_B = s(\theta = 1/2, T = 0)/k_B = s(\theta = 3/4, T = 0)/k_B = 0$. These marked

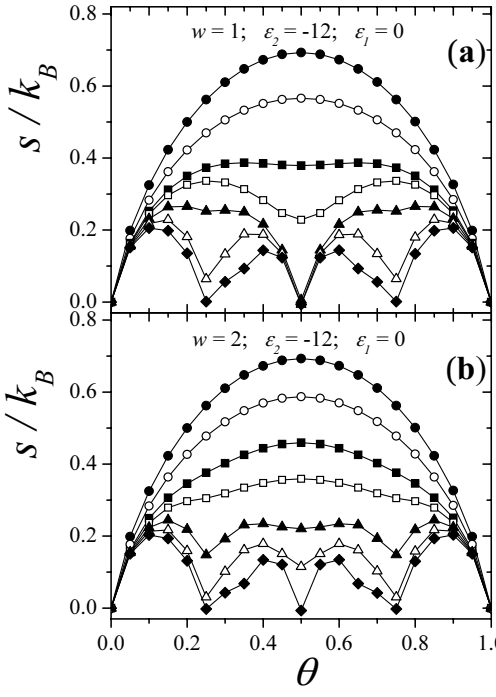

Fig. 16. Configurational entropy per site (in units of k_B) versus the surface coverage for interacting particles adsorbed in chessboard substrates with $l = 12$ and $\Delta\varepsilon = 12$. The curves from top to bottom correspond to different temperatures: full circles, $k_BT = \infty$; open circles, $k_BT = 4.90$; full squares, $k_BT = 2.48$; open squares, $k_BT = 1.66$; full triangles, $k_BT = 0.67$; open triangles, $k_BT = 0.40$, and full diamonds, $k_BT = 0.20$. (a) $w = 1$ and (b) $w = 2$.

singularities are separating four different adsorption processes: (i) for $0 < \theta < 1/4$, the strong site patches are filled until the $c(2\times2)$-ordered phase is formed on them; (ii) for $1/4 < \theta < 1/2$, the filling of the strong site patches is completed; (iii) for $1/2 < \theta < 3/4$, the weak site patches are filled until the $c(2 \times 2)$-ordered phase is formed on them; (iv) for $3/4 < \theta < 1$, the filling of the weak site patches is completed. The appearance of $c(2 \times 2)$ structures in the patches is related to the well-known order–disorder phase transition occurring in a repulsive lattice gas at low temperatures.[86]

We now analyze the case corresponding to $w = 4$ [Fig. 17(a)] and $w = 5$ [Fig. 17(b)]. As shown in Fig. 16, three minima appear in the entropy as T decreases. Nevertheless, the cause of these minima in Figs. 17(a) and 17(b) is different. In fact, the filling of the lattice proceeds according to the following processes: (i) for $0 < \theta < 1/4$, the strong site patches are filled until the $c(2\times2)$-ordered phase is formed on them; (ii) for $1/4 < \theta < 1/2$, the weak site patches are filled until the $c(2 \times 2)$-ordered phase is formed on them; (iii) for $1/2 < \theta < 3/4$, the filling of the strong site patches is completed; (iv) for $3/4 < \theta < 1$, the filling of the weak site patches is completed.

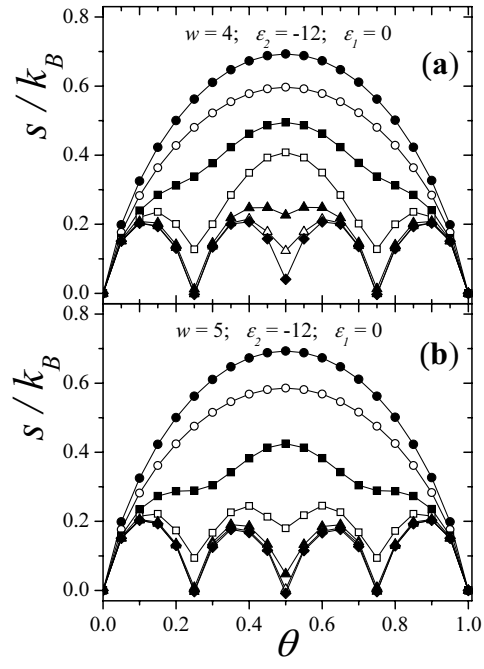

Fig. 17. Configurational entropy per site (in units of k_B) versus the surface coverage for interacting particles adsorbed in chessboard substrates with $l = 12$ and $\Delta\varepsilon = 12$. The curves from top to bottom correspond to different temperatures: full circles, $k_BT = \infty$; open circles, $k_BT = 4.90$; full squares, $k_BT = 2.48$; open squares, $k_BT = 1.66$; full triangles, $k_BT = 1.00$; open triangles, $k_BT = 0.67$, and full diamonds, $k_BT = 0.20$. (a) $w = 4$ and (b) $w = 5$.

As it can be easily understood, as long as the condition $w/\Delta\varepsilon < 1/4$ is satisfied, the adsorption process is similar to the one described in Fig. 16, i.e., strong site patches are filled first and weak site patches are filled after. We call this feature Regime I (RI). On the other hand, as $w/\Delta\varepsilon > 1/3$ the adsorption process is shown in Fig. 17, which we call Regime II (RII). In this case, both patches are filled sequentially.

In the next figure, we show RI and RII from a new perspective. For this purpose, Fig. 18(a) [Fig. 18(b)] presents a typical low-temperature adsorption isotherm (coverage versus chemical potential, μ) in RI (RII). As can be observed, the partial densities, θ_1 and θ_2, which are associated with sites with energy ε_1 and ε_2, show competition between easily visualized by following the behavior of θ_1 and θ_2.

It should be noted that Regimes I and II are disconnected. In between, i.e., $1/4 \leq w/\Delta\varepsilon \leq 1/3$, the system behaves in a mixed transition regime changing continuously from one to another.

An interesting case occurs for $w = 3$ (Fig. 19). For this value of the lateral interaction, the adsorption process is as follows: (i) the strong site patches are filled until the $c(2 \times 2)$-ordered phase is formed on them; (ii) for $0.25 < \theta < 0.75$, the particles can be adsorbed on strong patches (with energy $\varepsilon_2 + 4w = 0$) or on weak

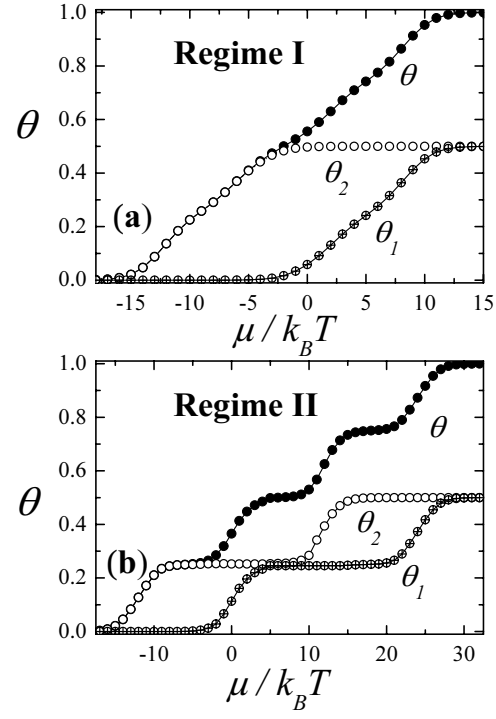

Fig. 18. Total and partial adsorption isotherms (coverage versus chemical potential μ) for a typical case in Regime I (top) and Regime II (bottom). Solid, dashed, and dotted lines represent total coverage θ, partial coverage of strong sites θ_1, and partial coverage of weak sites θ_2, respectively.

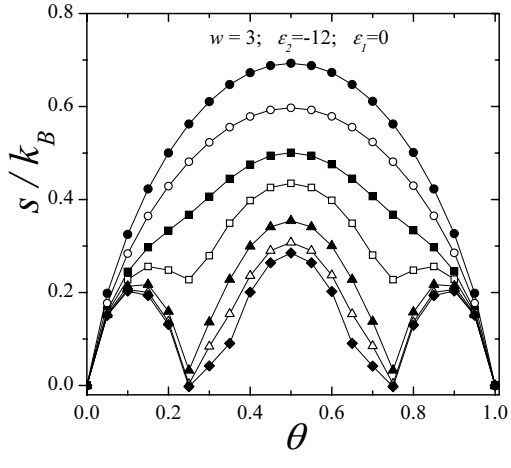

Fig. 19. Configurational entropy per site (in units of k_B) versus the surface coverage for interacting particles adsorbed in chessboard substrates with $l = 12$, $\Delta\varepsilon = 12$, and $w = 3$. The curves from top to bottom correspond to different temperatures: full circles, $k_BT = \infty$; open circles, $k_BT = 4.90$; full squares, $k_BT = 2.48$; open squares, $k_BT = 1.66$; full triangles, $k_BT = 1.00$; open triangles, $k_BT = 0.67$, and full diamonds, $k_BT = 0.20$.

sites (with energy $\varepsilon_1 = 0$). For this reason, the entropy varies smoothly between $0.25 < \theta < 0.75$, and the minimum at $\theta = 0.5$ disappears. The process (ii) concludes when the weak site patches are filled until the $c(2 \times 2)$-ordered phase is formed on them; and finally, (iii) the filling of the weak site patches is completed.

In the following, we will analyze what happens when the topography is changed. For this purpose, we fix the energies (lateral interaction and difference between the energies of the patches) and the temperature, and vary the size l of the patches. The result of this analysis is shown in Figs. 20 and 21 for RI and RII, respectively. It can be seen that all curves vary between two limit ones: the one corresponding

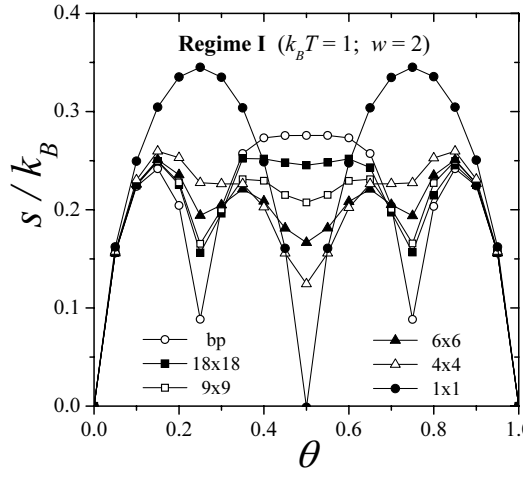

Fig. 20. Configurational entropy per site (in units of k_B) versus coverage for square chessboard topographies with different l's, $\Delta\varepsilon = 12$, $w = 2$, and $k_BT = 1$ (Regime I). The different values of l are displayed in the figure.

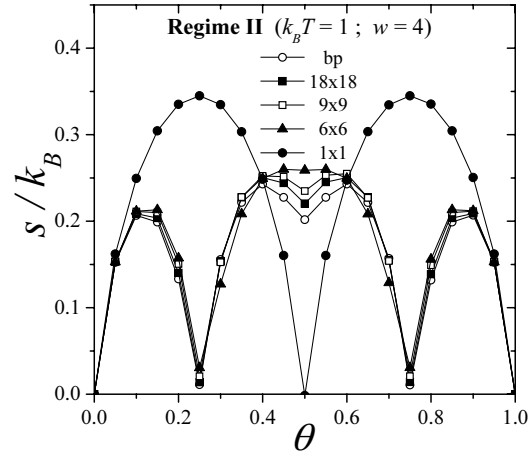

Fig. 21. Same as Fig. 20 for $w = 4$ and $k_BT = 1$ (Regime II).

to 1×1 patches and the one corresponding to *bp* (two big patches). The fact that the entropy for different topographies, characterized by a length scale l, varies between two extreme curves (see Figs. 20 and 21) suggests that we should search for some appropriate quantity to measure deviation among these curves and study the behavior of such quantity as the length scale is varied. The quantity we found most suitable is

$$\chi_s = \sum_i [s(\theta_i) - s^{bp}(\theta_i)]^2 \,, \tag{11}$$

where $s^{bp}(\theta_i)$ is the reference entropy and the sum runs over all values of coverage (between 0 and 1). The results for χ_s are shown in Fig. 22, where we can see that χ_s behaves as a power law in l with two different values of the exponent, α_s, depending on the ratio $w/\Delta\varepsilon$. These results confirm the existence of two adsorption regimes at low temperatures. A similar behavior was recently observed in Refs. 82 and 83 for other properties of adsorption (isotherms and differential heat of adsorption), which reinforce the robustness of the results presented here.

3.3. *Configurational entropy of interacting particles adsorbed on diluted-bond triangular lattices*

Now, we address the case of surfaces with geometric heterogeneity. The object of our study is the determination of the effects of geometric-quenched disorder of the substrate on the thermodynamics of adsorption of monomers, when the disorder is represented by a variable connectivity, as inspired by the problem of adsorption on the surface of amorphous solids. Thus, we consider monomers ($k = 1$) adsorbed on a diluted-bond triangular lattice (connectivity $z = 6$) with $M = L \times L$ sites and

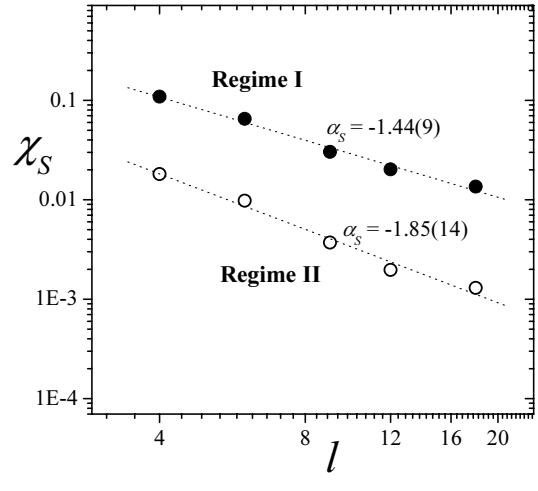

Fig. 22. Power law behavior of the quantity χ_S showing the data for chessboard topographies in RI and RII.

$m = 3M$ bonds, with periodic boundary conditions. Particles interact through a NN repulsive energy, $w > 0$. Then, the Hamiltonian of the system is given by Eq. (1) with $k = 1$. In addition, in the case of an energetically homogeneous surface, as the one to be considered here, all ε_i's are the same and we can take them equal to zero without loss of generality.

In general, we have used in our calculations $M \approx 10^4$ ($L \approx 100$). Care had to be taken in order to select the precise size, which would allow the formation of the ordered phases. The approach to thermal equilibrium is usually reached in $m = 10^5$ MCS, after that the mean value of U at a given temperature is calculated as a simple average over $m' = 10^5$ additional MCS. Then, the entropy is obtained from Eqs. (2)–(4). As in previous sections, the entropy per site will be used. Given that our system is disordered, it is important to stress that all the above calculations are repeated over 100 replicas of the system for each fixed degree of disorder and all thermodynamical quantities are finally averaged over them.

The case $\rho = 0$ corresponds to the completely ordered system (homogeneous triangular lattice) and was discussed in Fig. 5. As some of the bonds are randomly deleted in the lattice, this becomes disordered with $\rho > 0$ and $z_{\text{mean}} < z$. Entropies for different values of ρ and w/k_BT are shown in Fig. 23. Curves from top to bottom correspond to different interaction strengths: full circles, $w/k_BT = 1$; open circles, $w/k_BT = 2$; full squares, $w/k_BT = 3$; open squares, $w/k_BT = 4$; full triangles, $w/k_BT = 5$; and open triangles, $w/k_BT = 6$. It can be observed that for high values

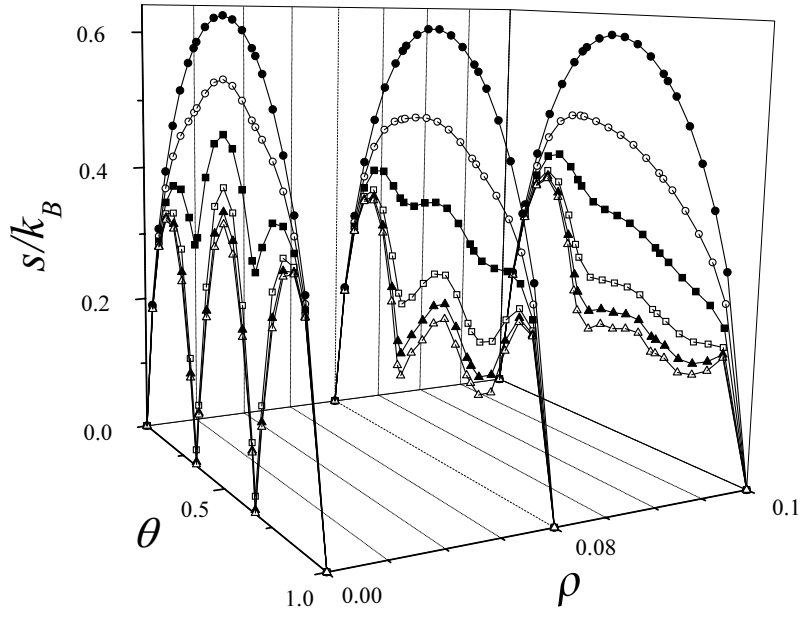

Fig. 23. Entropy per site for triangular lattices with different degrees of disorder and for different interaction strengths: full circles, $w/k_BT = 1$; open circles, $w/k_BT = 2$; full squares, $w/k_BT = 3$; open squares, $w/k_BT = 4$; full triangles, $w/k_BT = 5$; and open triangles, $w/k_BT = 6$.

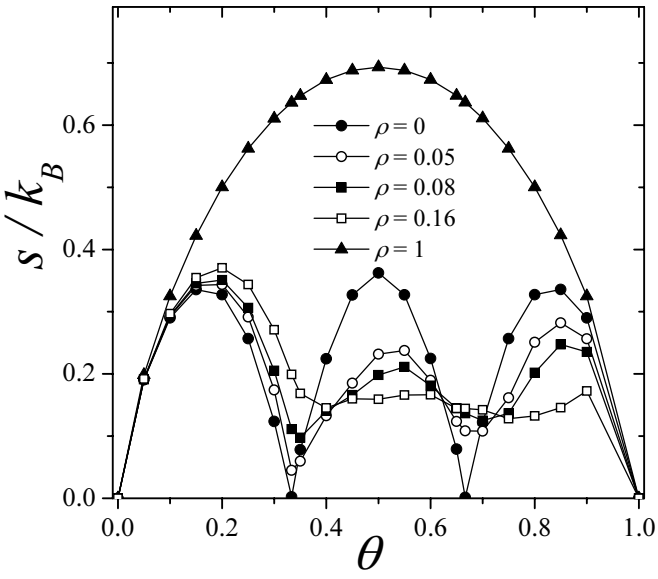

Fig. 24. Entropy per site for triangular lattices with different degrees of disorder (as indicated) at a fixed interaction strength ($w/k_BT = 6$).

of w/k_BT the minima in the entropy are gradually smeared out as ρ increases. In addition, the particle-vacancy symmetry is lost. This can be better appreciated in Fig. 24, where the above thermodynamical quantities are represented for a fixed high value of w/k_BT ($w/k_BT = 6$) and increasing values of the degree of disorder. This symmetry breaking can be explained by taking into account the fact that, due to repulsive interactions, sites attached to deleted bonds will be filled preferentially as the coverage increases.

The above results suggest the existence of a critical degree of disorder ρ_c (critical mean connectivity z_c), below (above) which the order–disorder phase transition observed for the ordered lattice will survive. In what follows, we explore in more details this possibility and work out a way of estimating these critical values and the extent to which the critical temperature is affected by the degree of disorder.

To estimate the variation of the critical temperature with the degree of disorder, we analyze the behavior of the entropy as a function of k_BT/w for different values of ρ. This method, suggested in Ref. 87 and later validated by finite-size scaling (FSS) analysis in Ref. 88, indicates that the position of the peak in ds/dT gives a good approximation of the critical temperature. The variation of s and ds/dT with temperature for different values of ρ is given in Figs. 25(a) and 25(b), respectively. We find that k_BT_c/w starts from the value 0.34 (close to the exact value of 0.3354) for $\rho = 0$ and then decreases appreciably as ρ increases (see Table 2).

The transition around $\theta = 2/3$ turns out to be much more sensitive to the degree of disorder. After performing the same studies as for $\theta = 1/3$, see Fig. 26, we find $\rho_c = 0.003$, or $z_c = 5.982$, and that k_BT_c/w starts from the value 0.34

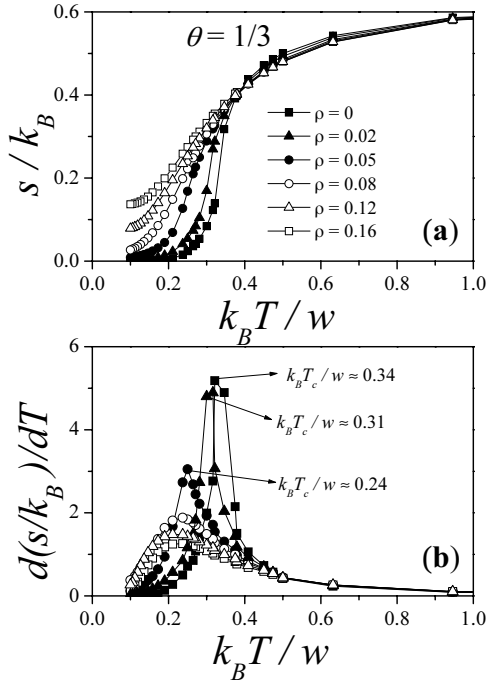

Fig. 25. Entropy per site (a) and its derivative (b), as a function of the interaction strength for lattices with different degrees of disorder (as indicated), at the low-coverage phase transition $\theta = 1/3$.

Table 2. Variation of the critical temperature for different degrees of disorder at the low- and high-coverage phase transitions.

	k_BT_c/w_T	
ρ	$\theta = 1/3$	$\theta = 2/3$
0.00	0.34	0.34
0.01	—	0.31
0.02	0.31	0.29
0.05	0.24	—

(close to the exact value of 0.3354) for $\rho = 0$ and decreases rapidly as ρ increases (see Table 2). It is therefore clear that critical parameters are different at the two phase transitions located at $\theta = 1/3$ and $2/3$, the latter being more sensitive to the degree of disorder, meaning that, at the same value of k_BT/w, the higher coverage transition disappears at a lower value of ρ and the critical temperature decreases faster with ρ. The reason of this behavior can be traced down to the particularities of the geometry of each ordered phase. At $\theta = 1/3$ the ordered phase consists of

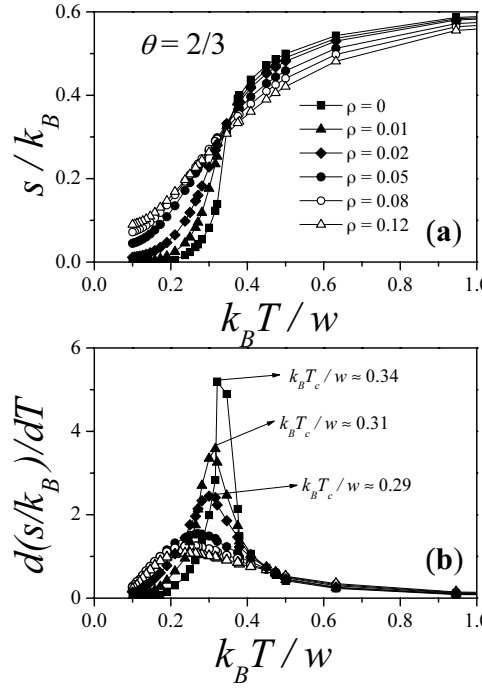

Fig. 26. Same as Fig. 25 for $\theta = 2/3$.

a configuration where any central filled site is surrounded by an hexagon with six empty sites at the corners. If just one bond between a filled and an empty site is eliminated, no new configurations arise with the same or lower energy. At $\theta = 2/3$, on the contrary, the ordered phase is characterized by the fact that any central empty site is surrounded by an hexagon with six filled sites at the corners. If just one bond between a filled and an empty site is eliminated (a radial bond in an hexagon), there are several new configurations with lower energy, namely those where the eliminated bond is transformed into one of the sides of an hexagon of filled sites. The system will try to evolve toward one of the new configurations passing through a huge number of intermediary partially disordered states.

The simple analysis performed here, although approximate, provides qualitative evidence about the critical behavior of the system. A more detailed and accurate study of this behavior, including the determination of the phase diagram and the variation of critical exponents, is being undertaken through FSS analysis.

3.4. *Configurational entropy for adsorbed linear species (k-mers)*

The knowledge of thermodynamic properties and phase behavior of interacting polyatomic lattice gases is still limited, and it is a developing field of research in gas–solid interface science. An early seminal contribution to dimer statistics was done by Fowler and Rushbrooke,[89] while an isomorphous system, namely adsorption

of binary liquid in two dimensions, was treated by Flory.[18,19] The thermodynamics of dimers was made for partially[90–97] and full coverage lattice[98–110] using exact and approximate methods. More recently, general results on thermodynamics and transport for noninteracting polymers in low-dimensional lattices were presented.[24] On the other hand, mean-field and quasi-chemical approximations were used to study the two-dimensional case.[111]

The structural ordering of interacting dimers has been analyzed by Phares *et al.*[110] The authors calculated the entropy of dimer on semi-infinite $M \times N$ square lattice ($N \to \infty$) by means of transfer matrix techniques. They concluded that there are a finite number of ordered structures. As it arose from simulation analysis,[112] only two of the predicted structures survive at thermodynamic limit. In fact, in Ref. 112, the analysis of the phase diagram for repulsive NN interactions on a square lattice confirmed the presence of two well-defined structures: a $c(4 \times 2)$-ordered phase at $\theta = 1/2$ and a "zig-zag" (ZZ) order at $\theta = 2/3$, being θ the surface coverage.

The thermodynamic implication of such a structural ordering was demonstrated through the analysis of adsorption isotherms[113] and the collective diffusion coefficient.[114] Later, MC simulations and FSS techniques have been used to study the critical behavior of repulsive linear k-mers in the low-coverage ordered structure (at $\theta = 1/2$).[88,115] A $(2k \times 2)$-ordered phase, characterized by alternating lines, each one being a sequence of adsorbed k-mers separated by k adjacent empty sites, was found. The critical temperature and critical exponents were calculated. The results revealed that the system does not belong to the universality class of the two-dimensional Ising model. The study was extended to triangular lattices.[55] In this case, the exponents obtained for $k > 1$ and $\theta = k/(2k+1)$ are very close to those characterizing the critical behavior of k-mers ($k > 1$) on square lattices at $\theta = 1/2$.

Here, we deal with attractive as well as repulsive k-mers adsorbed on regular lattices of $M = L \times L$ adsorptive sites, where L is the linear size of the array. The k-mers can only adsorb flat on the surface occupying k lattice sites. Only NN units of different k-mers interact through an interaction energy w. Then, the Hamiltonian of the system is given by Eq. (1) with $b_{ij} = 1 \; \forall \langle i,j \rangle$ and $\varepsilon_i = \varepsilon_0 = 0 \; \forall i$ (homogeneous surface).

The entropy per site was calculated by following the method of the artificial Hamiltonian described in Sec. 2.2. The temperature dependence of $u_A(T)$ and $u(T)$ was obtained by MC simulation in the canonical ensemble. A typical curve $u(T)$ is depicted in Fig. 3 for repulsive dimers on a square lattice (full circles). Integration through Eq. (7) was carried out by standard methods after spline-fitting u_A and u versus T, respectively.

Results of thermodynamic integration with an artificial reference system are shown in Fig. 27 for attractive dimers in a one-dimensional lattice. The high accuracy of this calculations can be asserted by comparison with exact analytical

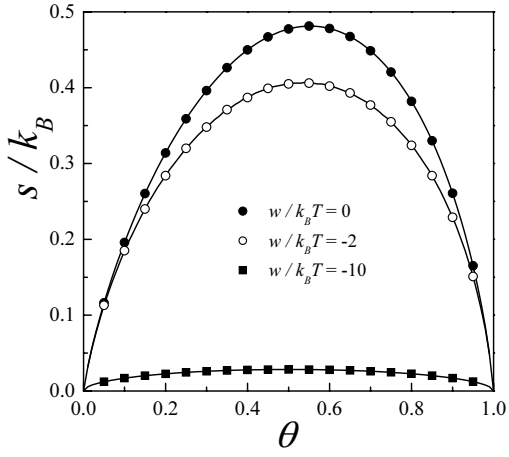

Fig. 27. Entropy per site (in units of k_B) versus surface coverage for attractive dimers in one dimension. Curves from top to bottom correspond to different values of w/k_BT as indicated. Solid lines represent data from Eq. (12). Calculations from thermodynamic integration with an artificial Hamiltonian as described in this work are shown in full circles.

ones for $s(\theta, T)$ recently presented in Ref. 116 (shown in full line). The formula for entropy per site of interacting k-mers is[116]

$$\frac{s(\theta,T)}{k_B} = \frac{\theta}{k}\ln\frac{\theta}{k} + (1-a)\ln(1-a) - 2a\ln a - \left[\frac{\theta}{k} - a\right]\ln\left[\frac{\theta}{k} - a\right] - (1-\theta-a)\ln(1-\theta-a) \tag{12}$$

and

$$a = \frac{2\theta(1-\theta)}{k\left[1 - \dfrac{(k-1)}{k}\theta + b\right]}, \quad b = \left\{\left[1 - \frac{(k-1)}{k}\theta\right]^2 - \frac{4}{kA}(\theta - \theta^2)\right\}^{1/2}, \tag{13}$$

$$A = [1 - \exp(-w/k_BT)]^{-1}. \tag{14}$$

A remarkable agreement is obtained as shown in Fig. 27. The behavior of repulsive dimers is reproduced throughout by the calculations of this work (as shown in Fig. 28) for all the ratios w/k_BT investigated. The local minimum of the entropy at $\theta = 2/3$ for strongly repulsive dimers is very well reproduced. This minimum corresponds to the developing of an ordered structure of alternating dimers as temperature decreases (see inset in Fig. 28). However, this minimum does not correspond to a phase transition as expected for a one-dimensional lattice gas with short-ranged interactions.

Equilibrium thermodynamics of k-mer lattice gases in two dimensions is a challenging theoretical problem with applications to adsorption of polyatomic molecules on surfaces. In the simplest case of interacting dimers, a very limited knowledge

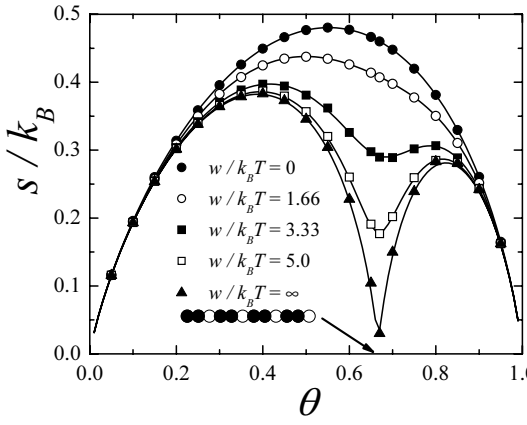

Fig. 28. Entropy per site (in units of k_B) versus surface coverage for repulsive dimers in one dimension. Curves from top to bottom correspond to different values of w/k_BT as indicated. Same as Fig. 27 for lines and symbols.

about its phase behavior is currently available.[110,112] By applying the method presented here, an accurate thermodynamic description of attractive and repulsive dimers in two dimensions can be accomplished.

For calculations of dimers entropy in a square lattice, a lattice size $M = 96 \times 96$ was used. A detailed analysis of finite-size effects (not shown here for the sake of shortness) concluded that lattices of this typical size are appropriate to give results representative of the thermodynamic limit within 1% of uncertainty. The results shown and discussed below correspond to dimers (Fig. 29) and trimers (Fig. 30) on a square lattice.

For noninteracting as well as attractive dimers, $s(\theta, T)$ has a maximum at $\theta > 0.5$. The overall effect of interactions is to decrease the entropy for all coverage. All these characteristics match the behavior of dimers in one dimension.[116] For repulsive dimers, $s(\theta, T)$ develops two local minima at $\theta = 1/2$ and $2/3$ as T decreases. In the ground state, $s(1/2, 0) = s(2/3, 0) = 0$. These values correspond to a (4×2) (see left inset in Fig. 29) and ZZ (see right inset in Fig. 29) ordered phases of dimers, respectively. The critical temperatures corresponding to the critical densities $\theta = 1/2$ and $2/3$ were estimated to be $T_c(1/2) \approx 0.33w/k_B$ and $T_c(2/3) \approx 0.20w/k_B$, in very good agreement with the values reported in Ref. 112 from finite-size analysis of order parameter cumulants. Our results confirm that only two out of the multiple minima arising from transfer matrix approximation for $s(\theta, T)$ of Phares *et al.*[110] are relevant.

Linear trimers exhibit an intriguing behavior (see Fig. 30 where $s(\theta, T)$ for noninteracting and repulsive straight and bended trimers are shown). From the comparison between noninteracting dimers and straight trimers in Figs. 29 and 30, it arises that the maximum of $s(\theta, T)$ slightly approaches $\theta = 1/2$ from above as the k-mer size increases. For repulsive straight trimers, two minima appear. Other

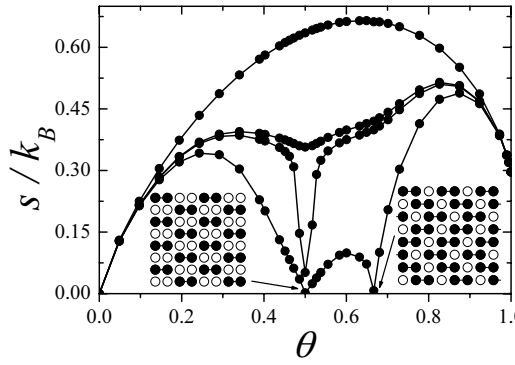

Fig. 29. Entropy per site (in units of k_B) versus surface coverage for repulsive dimers in two dimensions. Curves from top to bottom correspond to $w/k_BT = 0$; $w/k_BT = 2.94$; $w/k_BT = 3.13$; and $w/k_BT = \infty$, respectively. In this figure, lines connecting symbols are included for better visualization; however, they do not correspond to theoretical results as they do in Figs. 27 and 28.

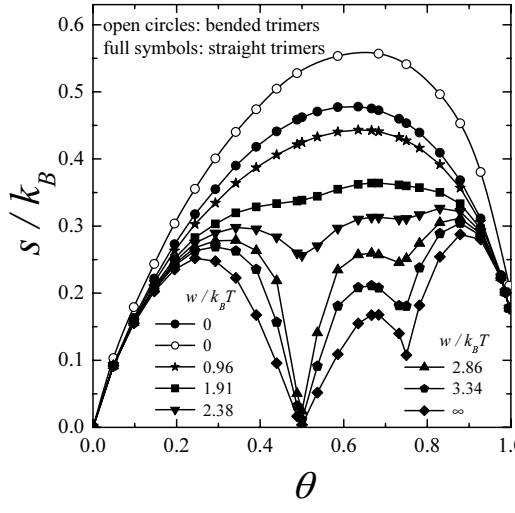

Fig. 30. Entropy per site (in units of k_B) versus surface coverage for bended (L-shape) and straight repulsive trimers in two dimensions. Curves with full circles from top to bottom correspond to straight trimers with different values of w/k_BT as indicated. Open circles correspond to bended trimers with $w/k_BT = 0$. Same as Fig. 29 for lines and symbols.

than the one at $\theta = 1/2$ with $s(1/2, 0) = 0$ corresponding to an (6×2)-ordered phase, it appears a very degenerate state with $s(3/4, 0) =$ finite at $\theta = 3/4$. This degeneracy remains as the ratio $w/k_BT \to \infty$ owing to the fact that trimers at this coverage can locally rearrange without any energy cost. This rearrangement is not possible for dimers in the ZZ phase at $\theta = 2/3$ and it makes a qualitative difference between the two cases. Whether this minimum trace to an order–disorder phase transition is still unknown.

The fact that trimers can have a bended configuration make a significant influence on its configurational entropy. As displayed in Fig. 30 for a pure phase of noninteracting bended trimers, $s(\theta, T)$ increases up to 20% at intermediate coverage with respect to a pure phase of straight trimers. The maximum also shifts appreciably to a higher coverage. Further analysis on the phase behavior, nature of phase transitions, and critical parameters is necessary in this case.

4. Conclusion

In summary, an interesting computational methodology has been presented for the calculation of the configurational entropy in generalized lattice gas models. The technique is based on the well-known TIM, along with a general definition of artificial Hamiltonians for discrete systems. Comparisons with rigorous analytical results demonstrate the method accuracy. This level of detail and accuracy cannot be ascertained by analytical approximations at the present. The methodology is a reliable strategy to gain insight into the critical properties and phase behavior of a wide variety of systems. In this sense, four applications have been discussed in this review.

In the first case, we have calculated the configurational entropy of an adlayer of interacting particles adsorbed in one-dimensional channels arranged in a triangular structure. Two kinds of lateral interaction energies have been considered: w_L, interaction energy between NN particles adsorbed along a single channel; and w_T, interaction energy between particles adsorbed across NN channels. We focused on the case of repulsive transversal interactions among adsorbed particles ($w_T = 1$), in such a way that the system was characterized by two nondimensional parameters w_L and k_BT. On this basis, different behaviors were observed: (i) for $w_L = 0$, successive transversal planes are uncorrelated and the system is equivalent to the well-known triangular lattice in two dimensions; consequently, two well-defined ordered structures are found at $\theta = 1/3$ and $\theta = 2/3$; (ii) for $w_L > 0$, the adlayer behaves as a three-dimensional fluid and a new structure is observed at $\theta = 0.5$; and (iii) for $w_L < 0$, two minima are observed in the configurational entropy. This is due to the fact that the ordered phases at $\theta = 1/3$ and $2/3$ are reinforced and extend along the channels.

In addition, an approximate estimation of the critical temperatures, corresponding to the critical concentrations $\theta = 1/3$, $1/2$, $2/3$, was obtained from the curves of configurational entropy as a function of the temperature.

In the second case, we have used the bivariate trap model in order to study how the surface topography affects the configurational entropy of repulsively interacting particles. In the framework of this model, it is assumed that the surface is formed by a collection of homogeneous patches. Every adsorptive site within a given patch has the same adsorptive energy. However, different patches have different adsorptive energies. We have considered only two kinds of square patches with different

energies, i.e., strong and weak patches, which are arranged in a chessboard-like ordered structure.

In order to analyze the effects of the topography on the configurational entropy of the adsorbate, three quantities have been chosen as the control parameters: (i) the relationship between the lateral interaction and the difference between the energies of the patches ($w/\Delta\varepsilon$); (ii) the temperature, and (iii) the size of the patches, l, which is associated with the correlation length. On this basis, different cases have been observed: (1) for high temperatures, the thermal energy governs the adsorption process and the entropy tends to the Langmuir case; (2) as the temperature decreases, the configurational entropy develops three minima at coverage $\theta = 1/4$, $1/2$, and $3/4$, which tend to zero in the ground state ($T = 0$). Depending on the value of $w/\Delta\varepsilon$, two different regimes are observed. For $w/\Delta\varepsilon < 1/4$ (Regime I), the strong sites patches are filled first and weak site patches are filled after. On the other hand, for $w/\Delta\varepsilon > 1/3$ (Regime II), both patches are filled sequentially up to 50%, and then, the filling of the patches is completed up to full coverage; and (3) for fixed energies and T, the configurational entropy appears as a very sensitive quantity to the correlation length, confirming the importance of the energetic correlation length as a controlling parameter in the adsorption process. This effect has been discussed in previous studies involving different process taking place on strong correlated surfaces.[81–84]

In the third case, we have studied the configurational entropy of repulsively interacting monomers adsorbed on disordered triangular lattices. Disorder is introduced by randomly deleting a fraction of bonds, representing interactions between particles adsorbed at NN sites, leading to lattices with variable connectivity, as inspired by the problem of adsorption on amorphous solids. Two order–disorder phase transitions exist for the ordered lattice at $\theta = 1/3$ and $2/3$ when the temperature is below the critical value given by $k_B T_c/w = 0.3354$ and all thermodynamic quantities show a particle-vacancy symmetry around $\theta = 1/2$. As the degree of disorder increases this particle-vacancy symmetry is broken but the phase transitions survive up to a critical disorder value, which is higher for the low-coverage region than for the high-coverage one. Critical temperatures at the two transitions decrease with the degree of disorder, this decreasing being faster for the high-coverage region. The present results, based on an approximate critical analysis, open the perspective of more accurate studies to be undertaken on the basis of FSS in order to determine accurately the phase diagram of the system and the behavior of critical exponents.

Finally, novel features shown for dimer and trimer entropy are in favor of a very rich phase behavior of larger adsorbed particles. Similar calculations of free energy (coverage and temperature dependence) would allow a complete thermodynamic description of adsorption systems in presence of multisite occupancy.

Further applications to more complex problems in statistical physics, as fractional statistics lattice gases and generalized statistics, would in principle be feasible.

Acknowledgments

This work was supported in part by CONICET (Argentina) under project PIP 112-200801-01332; Universidad Nacional de San Luis (Argentina) under project 322000; and the National Agency of Scientific and Technological Promotion (Argentina) under project 33328 PICT 2005. The numerical works were done using the BACO parallel cluster (composed by 60 PCs each with a 3.0 GHz Pentium-4 processor) located at Instituto de Física Aplicada, Universidad Nacional de San Luis-CONICET, San Luis, Argentina.

References

1. A. Boutin, R. J.-M. Pellenq and D. Nicholson, *Chem. Phys. Lett.* **219**, 484 (1994).
2. V. Lachet, A. Boutin, R. J.-M. Pellenq, D. Nicholson and A. H. Fuchs, *J. Phys. Chem.* **100**, 9006 (1996).
3. R. Radhakrishnan and K. Gubbins, *Phys. Rev. Lett.* **79**, 2847 (1997).
4. T. Maris, T. J. H. Vlugt and B. Smit, *J. Phys. Chem.* **102**, 7183 (1998).
5. C. Martin, N. Tosi-Pellenq, J. Patarin and J. P. Coulomb, *Langmuir* **14**, 1774 (1998).
6. J. P. Coulomb, C. Martin, N. Floquet, Y. Grillet and J. Patarin, *Fundamentals of Adsorption, Proc. Sixth Int. Conf.*, ed. F. Meunier (Elsevier, Amsterdam, 1998), p. 165.
7. W. H. Weinberg, *Ann. Rev. Phys. Chem.* **34**, 217 (1983).
8. W. Rudziński and D. H. Everett, *Adsorption of Gases on Heterogeneous Surfaces* (Academic Press, London, 1992).
9. M. J. Jaroniec and R. Madey, *Physical Adsorption on Heterogeneous Surfaces* (Elsevier, Amsterdam, 1988).
10. W. Rudziński, W. A. Steele and G. Zgrablich, *Equilibria and Dynamics of Gas Adsorption on Heterogeneous Solid Surfaces* (Elsevier, Amsterdam, 1996).
11. E. I. Benegas, V. Pereyra and G. Zgrablich, *Surf. Sci.* **187**, L647 (1987).
12. W. A. Steele, *Langmuir* **15**, 6083 (1999).
13. R. Zallen, *The Physics of Amorphous Solids* (Wiley, New York, 1998).
14. M. Fähnle, *J. Phys. C: Solid State Phys.* **16**, L819 (1983).
15. G. Mazzeo and R. Kühn, *Phys. Rev. E* **60**, 3823 (1999).
16. S. Galam and P. V. Koseleff, *Eur. Phys. J. B* **28**, 149 (2002).
17. W. Janke and M. Weigel, in *High Performance Computing in Science and Engineering*, Transactions of the Second Joint HLRB and KONWIHR Result and Reviewing Workshop, March 2–3, 2004, Technical University of Munich (Springer-Verlag, Berlin, 2005), p. 363–373.
18. P. Flory, *J. Chem. Phys.* **10**, 51 (1942).
19. P. Flory, *Principles of Polymer Chemistry* (Cornell, Ithaca N. Y., 1953).
20. M. L. Huggins, *J. Phys. Chem.* **46**, 151 (1942).
21. M. L. Huggins, *Ann. N. Y. Acad. Sci.* **41**, 151 (1942).
22. M. L. Huggins, *J. Am. Chem. Soc.* **64**, 1712 (1942).
23. E. A. Guggenheim, *Proc. R. Soc. Lond. A* **183**, 203 (1944).
24. A. J. Ramirez-Pastor, T. P. Eggarter, V. D. Pereyra and J. L. Riccardo, *Phys. Rev. B* **59**, 11027 (1999).
25. F. Romá, A. J. Ramirez-Pastor and J. L. Riccardo, *Langmuir* **19**, 6770 (2003).
26. J. L. Riccardo, F. Romá and A. J. Ramirez-Pastor, *Phys. Rev. Lett.* **93**, 186101 (2004).
27. T. Nitta, M. Kuro-oka and T. Katayama, *J. Chem. Eng. Jpn.* **17**, 45 (1984).

28. T. Nitta and A. J. Yamaguchi, *J. Chem. Eng. Jpn.* **25**, 420 (1992).
29. J. L. Firpo, J. J. Dupin, G. Albinet, A. Bois, L. Casalta and J. F. Baret, *J. Chem. Phys.* **68**, 1369 (1992).
30. E. A. DiMarzio, *J. Chem. Phys.* **35**, 658 (1961).
31. P. M. Pasinetti, J. L. Riccardo and A. J. Ramirez-Pastor, *J. Chem. Phys.* **122**, 154708 (2005).
32. M. Quintana, M. Pasinetti, A. J. Ramirez-Pastor and G. Zgrablich, *Surf. Sci.* **600**, 33 (2006).
33. F. Romá and A. J. Ramirez-Pastor, *Physica A* **328**, 513 (2003).
34. F. Romá, A. J. Ramirez-Pastor and J. L. Riccardo, *Langmuir* **16**, 9406 (2000).
35. F. Romá, A. J. Ramirez-Pastor and J. L. Riccardo, *J. Chem. Phys.* **114**, 10932 (2001).
36. K. Binder, *Applications of the Monte Carlo Method in Statistical Physics. Topics in Current Physics*, Vol. 36 (Springer, Berlin, 1984).
37. J. P. Hansen and L. Verlet, *Phys. Rev.* **184**, 151 (1969).
38. K. Binder, *J. Stat. Phys.* **24**, 69 (1981).
39. K. Binder, *Z. Phys. B* **45**, 61 (1981).
40. K. K. Mon and K. Binder, *Phys. Rev. B* **42**, 675 (1990).
41. J. Yepez, *J. Stat. Phys.* **81**, 255 (1995).
42. F. Romá, A. J. Ramirez-Pastor and J. L. Riccardo, in *Adsorption Science and Technology*, ed. D. D. Do (World Scientific Publishing, Singapore, 2000), pp. 527–531.
43. S. K. Ma, *J. Stat. Phys.* **26**, 221 (1981).
44. Z. Alexandrowicz, *J. Chem. Phys.* **55**, 2765 (1971).
45. H. Meirovitch, *Chem. Phys. Lett.* **45**, 389 (1977).
46. J. P. Valleau and D. N. Card, *J. Chem. Phys.* **57**, 5457 (1972).
47. G. Torrie and J. P. Valleau, *Chem. Phys. Lett.* **28**, 578 (1974).
48. G. Torrie and J. P. Valleau, *J. Comput. Phys.* **23**, 187 (1977).
49. G. Torrie and J. P. Valleau, *J. Chem. Phys.* **66**, 1402 (1977).
50. Z. Salsburg, J. Jacobsen, W. Fickett and W. Wood, *J. Chem. Phys.* **30**, 65 (1959).
51. M. de Koning, A. Antonelli and S. Yip, *Phys. Rev. Lett.* **83**, 3973 (1999), and references therein.
52. N. Metropolis, A. W. Rosenbluth, M. N. Rosenbluth, A. H. Teller and E. Teller, *J. Chem. Phys.* **21**, 1087 (1953).
53. K. Hukushima and K. Nemoto, *J. Phys. Soc. Jpn.* **65**, 1604 (1996).
54. D. J. Earl and M. W. Deem, *Phys. Chem. Chem. Phys.* **7**, 3910 (2005).
55. P. M. Pasinetti, F. Romá, J. L. Riccardo and A. J. Ramirez-Pastor, *Phys. Rev. B* **74**, 155418 (2006).
56. K. K. Unger, D. Pan, A. Mersmann, Y. Grillet, F. Rouquerol and J. Rouquerol, in *Zeolites as Catalysts, Sorbents and Detergent Builders*, eds. H. G. Karge and J. Weitkamp (Elsevier, Amsterdam, 1989), pp. 625.
57. U. Müller, H. Reichert, E. Robens, K. K. Unger, Y. Grillet, F. Rouquerol, J. Rouquerol, D. Pan, A. Mersmann and Z. Fresenius, *Anal. Chem.* **333**, 433 (1989).
58. P. Llewellyn, J. P. Coulomb, Y. Grillet, J. Patarin, H. Lauter, H. Reichert and J. Rouquerol, *Langmuir* **9**, 1846 (1993).
59. P. Llewellyn, J. P. Coulomb, Y. Grillet, J. Patarin, G. André and J. Rouquerol, *Langmuir* **9**, 1852 (1993).
60. Y. Grillet, P. L. Llewellyn, N. Tosi-Pellenq and J. Rouquerol, in *Fundamentals of Adsorption, Proc. Fourth Int. Conf.*, ed. M. Suzuki (Kodansha Ltd., Tokyo, 1993), p. 235.
61. N. Tosi-Pellenq, Y. Grillet, J. Rouquerol and P. Llewellyn, *Thermochim. Acta* **204**, 79 (1992).

62. J. C. Martin, N. Tosi-Pellenq, J. Patarin and J. P. Coulomb, *Langmuir* **14**, 1774 (1998).
63. J. P. Coulomb, C. Martin, N. Floquet, Y. Grillet and J. Patarin, in *Fundamentals of Adsorption, Proc. Sixth Int. Conf.*, ed. F. Meunier (Elsevier, Amsterdam, 1998), p. 165.
64. M. R. Swift, E. Cheng, M. W. Cole and J. R. Banavar, *Phys. Rev. B* **48**, 3124 (1993).
65. R. Radhakrishnan and K. E. Gubbins, *Phys. Rev. Lett.* **79**, 2847 (1997).
66. M. W. Cole, V. H. Crespi, G. Stan, C. Ebner, J. M. Hartman, S. Moroni and M. Boninsegni, *Phys. Rev. Lett.* **84**, 3883 (2000).
67. R. A. Trasca, M. M. Calbi and M. W. Cole, *Phys. Rev. E* **65**, 061607 (2002).
68. R. A. Trasca, M. M. Calbi, M. W. Cole and J. L. Riccardo, *Phys. Rev. E* **69**, 011605 (2004).
69. M. M. Calbi and M. W. Cole, *Phys. Rev. B* **66**, 115413 (2002).
70. M. M. Calbi, S. M. Gatica, M. J. Bojan, G. Stan and M. W. Cole, *Rev. Mod. Phys.* **73**, 857 (2001).
71. M. M. Calbi and J. L. Riccardo, *Phys. Rev. Lett.* **94**, 246103 (2005).
72. L. Chen and J. K. Johnson, *Phys. Rev. Lett.* **94**, 125701 (2005).
73. J. V. Pearce *et al.*, *Phys. Rev. Lett.* **95**, 185302 (2005).
74. L. Heroux, V. Krungleviciute, M. M. Calbi and A. D. Migone, *J. Phys. Chem. B* **110**, 1297 (2006).
75. D. P. Landau, *Phys. Rev. B* **27**, 5604 (1983).
76. A. A. Tarasenko, F. Nieto, L. Jastrabík and C. Uebing, *Phys. Rev. B* **64**, 075413 (2001).
77. A. J. Ramirez-Pastor and F. Bulnes, *Physica A* **283**, 198 (2000).
78. P. M. Pasinetti, J. L. Riccardo and A. J. Ramirez-Pastor, *Physica A* **355**, 383 (2005).
79. F. Nieto, C. Uebing, V. Pereyra and R. Faccio, *Surf. Sci.* **423**, 256 (1999).
80. F. Nieto, A. J. Ramirez-Cuesta and R. Faccio, *Phys. Rev. E* **59**, 3706 (1999).
81. M. Nazzarro, F. Nieto and A. J. Ramirez-Pastor, *Surf. Sci.* **497**, 275 (2002).
82. F. Bulnes, A. J. Ramirez-Pastor and G. Zgrablich, *J. Chem. Phys.* **115**, 1513 (2001).
83. F. Bulnes, A. J. Ramirez-Pastor and G. Zgrablich, *Phys. Rev. E* **65**, 31603 (2002).
84. J. E. González and A. J. Ramirez-Pastor, *Physica A* **311**, 275 (2002).
85. T. W. Fishlock, J. B. Pethica and R. G. Egdell, *Surf. Sci.* **L47**, 445 (2000).
86. J. M. Yeomans, *Statistical Mechanics of Phase Transitions* (Clarendon Press, Oxford, 1992).
87. J. E. González, A. J. Ramirez-Pastor and V. D. Pereyra, *Langmuir* **17**, 6974 (2001).
88. F. Romá, A. J. Ramirez-Pastor and J. L. Riccardo, *Phys. Rev. B* **72**, 035444 (2005).
89. R. H. Fowler and G. S. Rushbrooke, *Trans. Faraday Soc.* **33**, 1272 (1937).
90. D. Lichtman and R. B. McQuistan, *J. Math. Phys.* **8**, 2441 (1967).
91. R. B. McQuistan, *Il Nuovo Cim. B* **58**, 86 (1968).
92. J. L. Hock and R. B. McQuistan, *J. Math. Phys.* **24**, 1859 (1983).
93. A. J. Phares, *J. Math. Phys.* **25**, 1756 (1984).
94. A. J. Phares, *J. Math. Phys.* **25**, 2169 (1984).
95. A. J. Phares, D. E. Shaw and F. J. Wunderlich, *J. Math. Phys.* **26**, 1762 (1985).
96. A. J. Phares and F. J. Wunderlich, *J. Math. Phys.* **26**, 2491 (1985).
97. A. J. Phares, F. J. Wunderlich, D. W. Grumbine and J. D. Curley, *Phys. Lett. A* **173**, 365 (1993).
98. P. W. Kasteleyn, *Physica* **27**, 1209 (1961).
99. P. W. Kasteleyn, *J. Math. Phys.* **4**, 287 (1963).
100. H. N. V. Temperley and M. E. Fisher, *Phil. Mag.* **6**, 1061 (1961).
101. M. E. Fisher, *Phys. Rev.* **124**, 1664 (1961).

102. J. F. Nagle, *Phys. Rev.* **152**, 190 (1966).
103. E. H. Lieb, *J. Math. Phys.* **8**, 2339 (1967).
104. D. S. Gaunt, *Phys. Rev.* **179**, 174 (1969).
105. O. H. Heilmann and E. H. Lieb, *Commun. Math. Phys.* **25**, 190 (1972).
106. A. J. Phares and F. J. Wunderlich, *J. Math. Phys.* **27**, 1099 (1986).
107. A. J. Phares and F. J. Wunderlich, *Il Nuovo Cim. B* **101**, 653 (1986).
108. D. J. Klein and T. G. Schmalz, *Phys. Rev. B* **41**, 2244 (1990).
109. K. W. Wojciechowski, D. Frenkel and A. C. Branka, *Phys. Rev. Lett.* **66**, 3168 (1991).
110. A. J. Phares, F. J. Wunderlich, J. D. Curley and D. W. Grumbine Jr., *J. Phys. A: Math. Gen.* **26**, 6847 (1993).
111. M. Dávila, F. Romá, J. L. Riccardo and A. J. Ramirez-Pastor, *Surf. Sci.* **600**, 2011 (2006).
112. A. J. Ramirez-Pastor, J. L. Riccardo and V. Pereyra, *Surf. Sci.* **411**, 294 (1998).
113. A. J. Ramirez-Pastor, J. L. Riccardo a nd V. Pereyra, *Langmuir* **16**, 10167 (2000).
114. A. J. Ramirez-Pastor, M. S. Nazzarro, J. L. Riccardo and V. Pereyra, *Surf. Sci.* **391**, 267 (1997).
115. F. Romá, A. J. Ramirez-Pastor and J. L. Riccardo, *Phys. Rev. B* **68**, 205407 (2003).
116. A. J. Ramirez-Pastor, A. Aligia, F. Romá and J. L. Riccardo, *Langmuir* **16**, 5100 (2000).